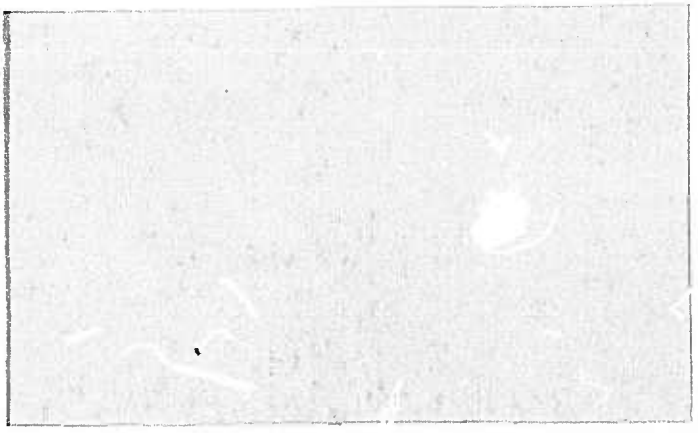

HYDRONAUTICS, incorporated research in hydrodynamics

Research, consulting, and advanced engineering in the fields of NAVAL and INDUSTRIAL HYDRODYNAMICS. Offices and Laboratory in the Washington, D. C. area: Pindell School Road, Howard County, Laurel, Md.

HYDRONAUTICS, Incorporated

TECHNICAL REPORT 7211-8

A LABORATORY STUDY OF WIND-WAVE-CURRENT INTERACTIONS

PART I

by

Richard S. Scotti

January 1975

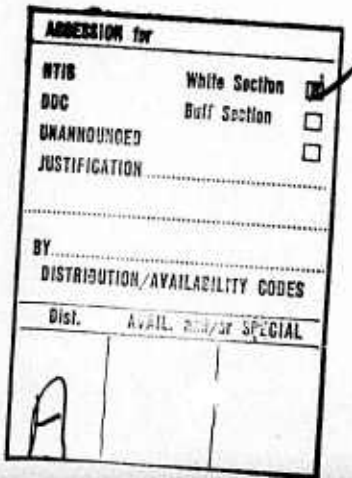

Sponsored by

Advanced Research Projects Agency
ARPA Order No. 1910, Amendment No. 5
Under
Contract N00014-72-C-0509
NR 062-472

UNCLASSIFIED

SECURITY CLASSIFICATION OF THIS PAGE (When Data Entered)

REPORT DOCUMENTATION PAGE

READ INSTRUCTIONS BEFORE COMPLETING FORM

1. REPORT NUMBER: Technical Report 7211-8
2. GOVT ACCESSION NO.:
3. RECIPIENT'S CATALOG NUMBER: (9)
4. TITLE (and Subtitle): A LABORATORY STUDY OF WIND-WAVE-CURRENT INTERACTIONS, PART I.
5. TYPE OF REPORT & PERIOD COVERED: Technical Report
6. PERFORMING ORG. REPORT NUMBER: T. R. 7211-8
7. AUTHOR(s): Richard S. Scotti
8. CONTRACT OR GRANT NUMBER(s): (15) N00014-72-C-0509 ARPA Order-1910
9. PERFORMING ORGANIZATION NAME AND ADDRESS: HYDRONAUTICS, Incorporated, 7210 Pindell School Road, Howard Co., Laurel, Maryland 20810
10. PROGRAM ELEMENT, PROJECT, TASK AREA & WORK UNIT NUMBERS: (16) NR-062-472
11. CONTROLLING OFFICE NAME AND ADDRESS: (11) Advanced Research Projects Agency, Arlington, Virginia 22209
12. REPORT DATE: January 1975
13. NUMBER OF PAGES: 75
14. MONITORING AGENCY NAME & ADDRESS (if different from Controlling Office): Office of Naval Research, Department of the Navy, Arlington, Virginia 22209 (12) 78p.
15. SECURITY CLASS. (of this report): Unclassified
15a. DECLASSIFICATION/DOWNGRADING SCHEDULE: None

16. DISTRIBUTION STATEMENT (of this Report)

This document has been approved for public release and sale; its distribution is unlimited.

17. DISTRIBUTION STATEMENT (of the abstract entered in Block 20, if different from Report)

(14) TR-7211-8

18. SUPPLEMENTARY NOTES

19. KEY WORDS (Continue on reverse side if necessary and identify by block number)

Wind Waves
Wind Drift Layer
Wave-Wave Interaction
Wind Wave Spectral Analysis

20. ABSTRACT (Continue on reverse side if necessary and identify by block number)

Two series of experiments were performed to study the interactions between both the wind-induced drift layer and the surface wave spectrum and a spatially varying subsurface current field. In the first, measurements were made of the response of the drift layer and surface wave spectrum to an appreciable, but unknown, current gradient. This was accomplished by forcing the current

DD FORM 1 JAN 73 1473 EDITION OF 1 NOV 65 IS OBSOLETE S/N 0102-014-6601

UNCLASSIFIED

SECURITY CLASSIFICATION OF THIS PAGE (When Data Entered)

174 500

20. Cont'd.

from a 90 cm-deep diffuser section onto a 68.7 cm-deep flat beach. The flow, thereby, experienced a current gradient which diminished to, and remained essentially at, zero a short distance downstream of the beach leading edge. The results in terms of the velocity difference across the drift layer differ from those for the wind-only case and will not admit to a simple Galilean transformation at the speed of the fluid below. Proceeding downwind, however, this difference decreases, giving evidence of an initial phase lag in the layer's response followed by a relaxation phenomenon. Relaxation times inferred from the data are on the order of 1 to 3 minutes. For the second test series, the beach was set at an angle of 2.65^{o} to produce strain rates in the range $10^{-3} \leq \partial Uc/\partial X \leq 10^{-2}$ (sec^{-1}). Here again, the results indicate that the response of the drift layer lags behind that of the current, as strained by the beach. The measurements of surface wave spectra taken for each of the conditions tested are presently being analyzed in detail; however, some preliminary results are presented.

TABLE OF CONTENTS

LIST OF FIGURES

LIST OF TABLES

ABSTRACT

Two series of experiments were performed to study the interactions between both the wind-induced drift layer and the surface wave spectrum and a spatially varying subsurface current field. In the first, measurements were made of the response of the drift layer and surface wave spectrum to an appreciable, but unknown, current gradient. This was accomplished by forcing the current from a 90 cm-deep diffuser section onto a 68.7 cm-deep flat beach. The flow, thereby, experienced a current gradient which diminished to, and remained essentially at, zero a short distance downstream of the beach leading edge. The results in terms of the velocity difference across the drift layer differ from those for the wind-only case and will not admit to a simple Galilean transformation at the speed of the fluid below. Proceeding downwind, however, this difference decreases, giving evidence of an initial phase lag in the layer's response followed by a relaxation phenomenon. Relaxation times inferred from the data are on the order of 1 to 3 minutes. For the second test series, the beach was set at an angle of 2.65 deg to produce strain rates in the range $10^{-3} \leq \partial Uc/\partial X \leq 10^{-2} (sec^{-1})$. Here again, the results indicate that the response of the drift layer lags behind that of the current, as strained by the beach. The measurements of surface wave spectra taken for each of the conditions tested are presently being analyzed in detail; however, some preliminary results are presented.

1. INTRODUCTION

Over the past ten years or so, the various aspects of the problem of the interaction between surface waves generated under the action of wind and subsurface current fields, such as produced by a train of progressive internal gravity waves, have been investigated in great detail. Areas of concentrated effort have included, for example, the generation of surface waves by wind, the dynamics of the surface waves themselves, the maintenance of surface waves by wind, the dynamics of internal waves, and the interactions between surface and internal waves. No doubt major steps have been taken both experimentally in isolating the phenomenon and studying the parts played by the various relevant parameters, and theoretically, in modeling the physics, and, thereby, offering predictions.

Still, the broad range and extremely variable nature of the flow condition encountered in the oceans make the problem all the more difficult and challenging. Theoretical models, which describe the observed interaction between wind-generated surface waves and internal waves propagating at comparable speeds, fail when the speeds are strongly disparate. Several mechanisms have been identified and each has its own merits; however, much yet remains to be done. Some highlights of the currently evolving models of and pressing questions relating to wind-wave-current interactions will be given here to rationalize the motivation for the present study.

Phillips[1] first considered the mechanism of blockage to account for the modifications that can be expected when a wind-generated wave field encounters a surface current disturbance associated with a train of internal waves. He showed that the surface waves will suffer significant modifications (or blockage) when the propagation speed of the internal wave pattern is approximately equal to half the phase velocity of the incident surface wave train, even if the disturbance velocity in the pattern is small. This effect has been observed experimentally in the laboratory demonstrating its reality. However, the actual flow field and the physics of wind-wave-current interactions are considerably more complex than admitted by Phillips' first model. In particular, no account was taken of the wind drift layer produced by the shear stress that exists at the air-water interface.

When the wind blows over the ocean, a shallow boundary layer flow is generated at the water surface. The effects involving this wind-induced drift layer are considered, generally, to be of two types: (1) Those in which the drift layer changes the surface wave dispersion, and (2) Those in which the drift layer itself is modified by the current field. Modeling the former case, Phillips[2] predicted that the presence of the drift layer will change the speed of propagation of even those surface waves whose wave lengths are large compared to the layer thickness. Changes in propagation speed in turn modify the interactions between the surface waves and a perturbing current field.

For the latter case, i.e., distortions of the drift layer itself, modulations of the surface wave field may be produced indirectly via modification of the drift layer. In this regard, Phillips[3] has derived a quantitative expression for the drift layer distortion that can occur when the length scale of the drift layer is small compared to that of the spartial variation of the perturbing current. His results, in terms of the velocity jump across the drift layer (i.e., the surface drift relative to the fluid below the layer), indicate that severe distortions, such as stagnation points on the surface and recirculating regions below, can be produced. The effects of viscosity, both molecular and turbulent, have been neglected in this analysis. Consequently, the drift layer's response to current perturbations (on a co-ordinate system moving with the internal wave pattern) must be steady in time and always in phase.

Vaglio-Laurin[4] has also considered the distortions produced in the wind drift layer due to a perturbing current. Including the effects of viscosity, he proposes that the response of the drift layer to fluctuations of the current will exhibit phase lags and relaxation which are characteristic of diffusive processes. Furthermore, significant distortion to the drift layer will be confined within a fraction of the layer's thickness below the surface. Vaglio-Laurin's model draws inspiration from an earlier work by Lighthill[5] on a laminar, viscous, unsteady boundary layer and from a study by Reynolds and Hussain[6] on the mechanics of an organized wave in turbulent shear flow.

Recently, Phillips[3] has developed a theoretical formulation for the modulations produced on short gravity waves by long waves, which are themselves being modulated by an internal-wave-induced current field. The problem of short wave modulation and breaking in the presence of long waves had already been taken up by Phillips and Banner[7]. They showed that non-linear modification of surface drift occurs near long wave crests and troughs to modulate the drift experienced by super-imposed short waves. One very important consequence of this effect would be to reduce the maximum amplitude that short waves can attain when they are at the point of incipient breaking near long wave crests. Phillips results suggest that the surface drift over a long wave can vary with respect to the phase of an attending internal wave (because the long wave amplitude varies) by as much as ten percent of the long wave speed. While only a small percentage of the long wave speed, this modulation represents a substantial fraction of the phase speed of the short waves riding on the long waves. Thus, significant changes of the energy density and propagation speed of short waves may be produced. The effects of viscosity have again been neglected so that perturbations in the current field will presumably be felt coherently across the local drift layer.

On the experimental side, the study by Lewis, Lake, and Ko[8] on the interaction of monochromatic surface and internal waves in a two fluid system is noteworthy. It provides valuable evidence in support of the resonance or blockage phenomenon as previously formulated by Phillips[1]. However, no wind (and,

hence, no wind generated surface drift layer) was included. The need for direct experimental measurements of wind-wave-current interactions is clear, for verifying as well as refining the results of the various theoretical models. In such interactions, what distortions, if any, are produced in the wind drift layer? Is the process diffusive or inviscid in nature? How is the surface wave spectrum modified and/or modulated by the presence of a subsurface current field? These questions, among those raised in a series of meetings conducted by ARPA last spring to coordinate theoretical and experimental efforts, are those to which the experimental test program reported herein has been addressed.

The experimental test program was conducted in two overlapping phases. In the first phase, modulations of the thin wind-drift layer by a perturbing current were measured by timing neutrally buoyant floats of several sizes between two fixed stations in the wind direction under the various test conditions. In the second phase, the effects of these interactions on the surface wave slope-spatial frequency spectra were measured utilizing the RRI TV camera system[9]. Simultaneously, capacitance wave-height probes were used to measure surface wave height-temporal frequency spectra. The results for the surface wave slope-spatial frequency spectra measurements will be reported on separately by Riverside Research Institute.

Section 2 contains a description of the experimental facility, the measurements taken and the operating characteristics. This same facility has been utilized in related studies over the past several years with only minor modifications.

There exists, therefore, a large amount of data and calibrations describing the operating conditions in the facility, given certain set-up parameters such as fan RPM, fetch, etc. We have drawn upon this existing information whenever possible, encouraged by spot checks and agreement with the present data.

In Section 3, the experiments are described and the results are presented. The important question of experimental accuracy for drift current measurements has been taken up as a necessary part of the present study. The results in the form of upper bounds on the expected standard deviations of the measurements are also presented here.

The results of measurements are discussed and summarized in Section 4. Concluding remarks are contained in Section 5, along with suggested guidelines for further investigation.

2. EXPERIMENTAL FACILITIES AND MEASUREMENTS

2.1 Wind-Wave-Current Facility

The HYDRONAUTICS wind-wave-current facility, shown schematically in Figure 1, is basically a 1.5 m-wide, 1.55 m-deep, and 22 m-long water tank. An axial flow fan, which is driven at an adjustable speed by an electric motor through a magnetic clutch, is located at the upstream end. To avoid the problem of wave reflections that would occur in any tank of finite length, a permeable wave absorber has been installed at the downstream end. A removable, sectional cover has been placed on the tank to create a wind tunnel 31 cms-high over a water depth of about 124 cms. Wind speeds up to 15 m/sec can be generated over the

water surface. The facility is also equipped with a variable current generation system also shown in Figure 1. The system consists of a false bottom or a submerged beach and a recirculating pump system, including a reversible impeller and appropriate ducting.

The primary flow variables in the facility are the wind speed and the artificial current direction, speed and streamwise gradient. The wind speed is controlled by the RPM of the fan. The current direction is, of course, determined by the sense of rotation of the impeller. The current gradient is controlled by the inclination of the beach as well as the magnitude of the current, while the current is directly related to the impeller RPM and the inclination of the beach. It is the current gradient that enables the simulation of certain key aspects of a moving current using a stationary current system, in that an equivalent internal wavelength or time-scale for a propagating current can be defined. It should be noted, however, that all measurements are hereby made relative to a coordinate system that effectively "rides" on a stationary internal wave. This point must be considered carefully before comparing the experimental laboratory data to other data or to theoretical predictions.

2.2 Measurements

2.2.1 Wind

The wind velocity profiles in the tunnel have been previously determined by vertical traverses of a pitot-static

tube supported on a precise motor-driven mechanism[10]. The tube was driven through the air stream at a constant speed of 2.5 cm/sec to measure the wind boundary layer near the water surface. A differential pressure transducer was used to sense the velocity head. Near, but not overly close to, the water surface the wind velocity profile was found to follow the logarithmic law. Friction velocities and roughness lengths were, thereby, inferred for many wind speeds and are presented in Figure 2. No such profiles were taken in the present experiments. The presence of a small (relative to the wind speed) favorable or adverse current no doubt effects the wind profile, and the value of U_*, as a modification of the boundary condition at the air-water interface. For small currents, this effect is felt to be small in regard to the establishment of U_* by the wind, even as the wave-dependent Stokes drift current represents only a small percentage of the wind-induced drift current in the fetch-limited laboratory[11]. In other words, the principal effect of a small subsurface current is felt to manifest itself as a modification of the surface wave spectrum with negligible change in the shear velocity. As the magnitude of the current is increased, however, the value of U_* increases or decreases depending on whether the current is adverse or favorable. This point of view is supported by the results of the present measurements within the drift layer and will be taken up again in Section 4. The results of Figure 2 were accepted as being approximately appropriate to the flow conditions of the present experiments.

2.2.2 Surface Wave Height and Frequency

A capacitance probe was used for wave measurements. The probe is made of a 0.13 mm-diameter, partially-submerged, Formvar-coated (a type of shellac that has good strength and electrical properties) copper wire acting as one electrode and a fully-submerged aluminum plate as the other. The change in capacitance of the wire with its depth of submergence is converted through an AC bridge circuit into a change in voltage, which can be maintained in a linear proportion over a useful depth range with suitable electronics. Within the frequency and spatial operating range of the probe, the output represents a trace of surface height as a function of time at a fixed point in space. It is possible, then, with the time history of surface height from a single probe (which in reality has been averaged over two-dimensional wave number space) to generate a wave height-temporal frequency spectrum. The probe output voltage was fed into an FM-tape recorder for storage to be processed at a later time or simultaneously into a visicorder for an immediate graphical display.

Previous studies by Wu[10] of the surface wave-height and frequency of the average or dominant waves under various wind conditions did not include the effects of subsurface current fields. His results are presented here, however, in Figure 3 to be used for comparison with the present data later on in this report.

2.2.3 Surface Drift Current

The drift current immediate to the water surface was measured by repeatedly timing floats of various sizes between two stations in the wind direction and then averaging over the results. Spherical particles with diameters of 1.90, 3.18, 6.35, 12.70 mm, and a specific gravity of 0.95 were used as floats. The velocity of each float was taken as the drift current at the depth of the centroid of the longitudinally projected area of the submerged portion of the float. For these floats used in the experiment, the corresponding centroid depths have been estimated (geometrically) to be 0.71, 1.19, 2.37, 4.72 mm, respectively. In some cases, two additional submerged floats (each constructed of a triangular wooden disk and a normal metal wire stem of the correct length to make the floats neutrally buoyant at the desired depth, see Reference 8) with centroid depths of 12.7 and 24.5 mm were also used. For many of the wind-current set-ups tested, use of these two deeper floats was impractical if not impossible. In particular, for cases with adverse subsurface currents, the drift layer profile connecting the downwind surface drift current to the upwind subsurface current has a zero crossing, typically in the depth range 12.7 to 25.4 mm. Under conditions of near-zero mean velocity and/or strong velocity gradients, the submerged floats did not perform well, and, therefore, were not used.

The efficiency of the timed-float technique has been demonstrated in many studies of the drift layer, including the present. Albeit cumbersome, time consuming, and unesthetic, no

better technique has been discovered as yet. Results of previous drift current measurements by Wu[10] for the case without subsurface currents are presented in Figure 4; included here, again, for the sake of comparison to the present data taken both with and without currents. The important questions of accuracy and reproducibility of results obtained with the timed-float technique will be considered in detail in Section 3.1.1.

2.2.4 Subsurface Currents

Subsurface currents produced by the current generation system were measured by timing the transport of nearly vertical dye streaks between two stations. Powdered dyes, Rhodamine (red), Alphazurine (blue), and Uranine (green), were mixed in cold tap water and simply poured into the stream at least one meter upstream of the measuring section. Observations indicated that below the first 2 to 4 cms of depth, wherein the dye dispersed very quickly owing to high turbulence levels, and extending down to at least 30 cms, the time-mean current was nearly uniform. Whenever possible, measurements were also taken of the transit time of small neutrally buoyant dirt particles in the flow between the same stations. In general, the results were in good agreement. As with the drift layer, measurements were repeated several times and averaged for both dye and dirt particle techniques.

The current flow below the surface drift layer was also quite unsteady, though not as turbulent as the surface layer, and under some of the conditions tested, exhibited a three-dimensional structure in the form of longitudinal and vertical

vortex tubes. These distortions were found to increase with increasing magnitude of current, to be worse for adverse currents (down the beach) than for favorable currents (up the beach), and to decrease with distance from the leading edge of the beach. All of these symptoms point to a poorly diffused and straightened recirculating current flow. In an investigation aimed at measuring a particular possible source of flow distortion, extraneous sources should, clearly, be avoided, or at least minimized. Thus, the recirculating current flow was considered to be inadequately diffused and straightened in the present set-up to provide reasonably smooth current fields for currents in excess of (approximately) ±15 cm/sec.

3. THE EXPERIMENT

3.1 Preliminary Considerations

3.1.1 Accuracy of Drift Layer Measurements

The efficiency of the timed-float technique for measuring the wind drift profile has been demonstrated in several previous HYDRONAUTICS' reports and has been accepted and successfully employed in several other outside experimental facilities. However, for the present experiment it was necessary to measure the change in the drift with and without a perturbing current field. To meet the obvious questions of accuracy and statistical confidence required for meaningful results, systematic experiments were first performed to optimize sample size and travel distance for minimum standard deviations. We expect for the case of zero current gradient that increasing either

sample size travel distance (for floats that travel in a reasonably straight path between the measuring stations) will decrease the measurement standard deviation. With a non-zero current gradient, on the other hand, the travel distance has to be below some value for meaningful estimates of the local drift velocity. For such tedious and time consuming measurements, some attempt at optimization was, clearly, in order.

To accomplish this end, float measurements for a series of relatively stringent flow conditions (with zero current gradient) were repeated many times (as many as 120) over different distances of float travel for each size float tested. The measurements were then grouped into different sized samples, i.e., samples per reading, and averaged to give a number of readings or "measurements." The standard deviation of the "measurements" was then computed and compared to that of the other groupings. Put in more concrete terms, the question we sought to answer was this: Given N samples of a measurement, to be separated into m groups of n samples each, and averaged over n, for what value of n will the standard deviation of the m groups be minimum? This study could more properly be termed an "educated optimization" in that "reasonable" values of float travel distance and of samples per measurement (n) were selected, based on experience, and statistics were computed and compared in the vicinity of these preselected values.

Trials were run with the beach in the horizontal position, the wind speed set at 6.7 m/sec (next to the highest speed tested), and for subsurface currents of 0, +9.2 cm/sec (favorable)

and -9.3 cm/sec (adverse). Float diameters (in mm) of 1.91, 3.18, 6.35, and 12.7, as well as a 25.4 mm-deep submerged float, were tested over travel distances of .5, .7, and 1.2 meters. The test conditions are summarized below:

Beach angle = 0^{o} (zero current gradient)
Wind speed = 6.67 m/sec
Subsurface current = -9.3, 0.0, +9.2 cm/sec
Float travel distance = .5, .7, 1.2 m
Float diameter = 1.91, 3.18, 6.35, 12.7 mm plus 25.4 mm-deep float
Trials, ranging from 15 to 120 each.

The number of samples per measurement (n) was taken as 5, 10, and 15 (and for a few cases, 20).

The results indicate that a float travel distance of 1.2 m and ten samples per measurement (the high and low are thrown out before averaging) yield the lowest standard deviations. These are presented, in part, in Table 1, where the standard deviations for the measurements are seen to vary inversely with float diameter, being generally larger for the smallest float. The largest standard deviations obtained are on the order of .5 to .6 cm/sec, which, relative to the mean velocity estimates, corresponds to only a 3 to 4 percent variation. It should be noted that the statistics no doubt vary as the test conditions are changed. However, these measurements which were taken with moderate wind speed and relatively strong currents are believed to provide reasonable estimates for the expected measurement uncertainties over all the flow conditions tested, including the case of small non-zero current gradient.

An additional factor yet to be mentioned is the presmoothing or filtering built right into the raw data. During the course of the experiments (in fact, for all experiments using the timed-float technique), those particles that pop out of and skip along the water surface, visibly dive down to lower, slower layers, or veer from the wind direction along the center of the tank by more than ±15 cms over the float travel distance, are ignored. The first two effects are more common with a water surface having large amplitude waves, not necessarily sharp crested, and are apparently related to the flow fields induced by the waves themselves. The latter effect is felt to be caused by three-dimensional structure within either the air stream or the subsurface current field. For example, large-scale, air-current fluctuations in the laboratory caused by the ventilation system or a suddenly opened or closed door would manifest themselves as vorticity in the wind stream. The three-dimensional structure in the current field has been already discussed briefly in an earlier section. The testing procedure during these trial runs was the same as that used during the experiments; the results are believed, therefore, to carry over.

The results of this preliminary study are important for the following two reasons: They prescribe an "optimized" test procedure by specifying float travel distance and number of float-trials per measurement. They provide estimates of the accuracy to be expected for each diameter float. Criteria of success, of course, lie with the quality of experimental data. As shall be discussed later on, when considering the measured data in detail,

the estimated accuracies appear to be quite realistic, if not a little conservative.

3.1.2 Selection of Test Conditions

The following theoretical guidelines as to the most useful and interesting test-flow conditions were supplied to us after the aforementioned ARPA organization meetings.

a. Wind speed, $U_W \leq 8$ m/sec, to which was added the lower limit of 2.85 m/sec below which the surface activity is small and difficult to measure quantitatively.

b. Subsurface current, U_c, both adverse and favorable,

$$-\frac{5}{4} \leq \frac{U_{D_o}}{U_{c\ max}} \leq +\frac{5}{4}$$

where U_{D_o} is the wind-induced surface drift velocity and $U_{c\ max}$ is the maximum current at the downwind end of the sloping beach.

Furthermore, the larger values were felt to be of special interest to enhance the anticipated perturbations and, thus, to facilitate the measurements. As previously discussed, the magnitude of $U_{c\ max}$ was constrained by consideration of flow geometry so that in some of the cases tested these limits were exceeded.

c. Strain rate, $\frac{1}{U_{c\ max}} \frac{\partial U_c}{\partial x} \leq 10^{-3} (cm^{-1})$. It is clear from the range of subsurface currents selected in

b. that the resonance phenomenon will probably not be an active mechanism here.

3.1.3 Matrix of Flow Conditions Tested

To date, two series of experiments have been performed. In the first, measurements were made, at two downwind stations, of the drift layer's response to an appreciable but unknown current gradient. This was accomplished by fixing the beach in the horizontal position at a depth of 68.7 cm. The current flow in passing from the 90 cm-deep diffuser section onto the beach, experiences a current gradient which diminishes to, and remained essentially at, zero a short distance downstream of the beach leading edge. The flat beach case is seen to simulate an infinitely long internal wave and the drift current, as measured along the beach, should then reflect the layer's response to an impulsive disturbance. Initially, data were obtained at stations 2 and 6; 138 and 381 cms from the leading edge, respectively, by measuring between stations 1-3 and 5-7 (see Figure 1). Data in this set is coded and referred to as B01. Another set of data, as part of the series for zero beach angle, was taken at stations 3 (202 cms from leading edge) and 6, in a manner similar to B01; this set is coded as B02. Surface wave spectra (both temporal-wave height and spatial-wave slope) were also measured in the latter set, B02.

For the second test series, the beach was set at an inclination from the horizontal of 2.65° to produce strain rates, $(1/U_{c\ max})(\partial U_c/\partial x) \leq 8 \times 10^{-4}(cm^{-1})$. Both drift layer profiles

and surface wave spectra measurements were taken at station 6 only. This test series is coded as B4.

The matrix of the flow conditions actually tested for each series is presented in Table 2 (a, b, and c).

3.2 Experimental Results

3.2.1 Flat Beach Series - Test Set B01

The results of measurements within the drift layer at an upstream and a downstream station along the flat beach for a moderate wind speed and both a favorable and an adverse current are shown in Figure 5 along with standard deviation bars. Presentation is in terms of q, the velocity relative to the fluid below, i.e., $q = U_D - U_c$. (U_D is the measured local drift velocity and U_c is the measured local current.) If the drift layer were everywhere in local equilibrium with the current field, the current would merely translate the layer in the Galilean sense. The data would thereby be collapsible onto one curve in terms of q. The results of Figure 5 indicate, however, that this is not the case.

It should be noted that the error bars given here were found to be quite realistic in that data runs repeated several days apart, while attempting to reconcile obvious distortions in these plots, consistently yielded results that fell within the bars. Reproducibility of data, therefore, while supporting the earlier estimates of measurement error also pointed out certain unexpected distortions in the meanflow. These distortions are believed to be the result of three-dimensional flow

structure, as previously mentioned, caused both by an inadequately diffused and straightened recirculating current flow and by flow separation from the beach-support struts.

After fairing smooth curves through the data at each station, as shown in Figure 5, differences were taken, at a fixed depth, between the results with and without current and are plotted versus distance along the beach in Figure 6. Here the differences are seen to diminish in the downstream direction. Interpreting the differences as phase lags in the drift layer's response to the current's history coming onto the flat beach, the observations strongly suggest a relaxation phenomenon. Estimates of a relaxation time constant, τ , were inferred using the results of Figure 6 and the relationship

$$(q - q_o)_{\text{downstream}} = (q - q_o)_{\text{upstream}} \, e^{-t/\tau}$$

where

$$t = \frac{\Delta x}{\overline{U}_{avg}} \quad ,$$

Δx = distance between stations 2 and 6, and

$\overline{U}_{avg}$ = average of the mean velocities at stations 2 and 6 at the given depth.

These are presented in Table 3(a) for each measurement depth.

The estimates of relaxation time are based on rather small differences between measurements taken at only two stations. Moreover, the results are also quite sensitive to the curves faired through the data points. These statements may be more

easily understood from a careful examination of Figures 5 and 6. Note in Figure 5 that estimates of τ are based on the separation between the curves at station (5-7), Figure 5(b), as compared to the separation at station (1-3), Figure 5(a). The quantitative details are presented in Table 3(a) and shown as a function of downwind position in Figure 6. The points in Figure 6 are connected by straight lines merely to indicate the trend of the data. Our assumption is, of course, that the data points lie on exponential curves. The expected standard deviation for each drift velocity measurement has already been given as roughly $\pm\frac{1}{2}$ cm/sec. If we apply this error range to the measurements listed in Table 3(a), where the differences on which τ is based are seen to vary from about 1.4 to 2.9 cm/sec, the computed magnitude of τ is formed to be uncertain by a factor ranging from $\frac{1}{2}$ to 10. Smoothness and reproducibility of the actual data, however, promise results that are much more reliable. That this is so is demonstrated below, especially when comparing results for different data runs. Still, we must view the calculated magnitudes of τ with these point in mind.

The results in Table 3(a) indicate that at a mean depth of 0.71 mm, at a wind speed of 6.67 m/sec, time constants of 48 and 21 seconds are appropriate for an adverse current of 9.3 cm/sec and for a favorable current of 9.2 cm/sec, respectively. The magnitude of τ is apparently constant with depth, except for the 4.7 mm position. At this depth (and below), the accuracy of the velocity differences, and especially of the mean drift velocity, used in the calculations falls off. Little

confidence is placed on the estimates of τ at the 4.7 mm depth and below. More will be said on this topic in the next section wherein the data from the more complete flat beach test set B02 is presented.

3.2.2 Flat Beach Series - Test Set B02

The second set of experiments performed with the beach in its horizontal position (B02) is distinguished from the first set (B01) on two counts

a. The upstream measuring station was moved downstream from station 2 for B01 to station 3 for B02. This change was made principally to accommodate the RRI TV system. However, the move was also justified to provide a longer flow transition length from the beach leading edge for the wider range of conditions tested in B02.

b. A period of 3 months elapsed between B01 and B02, during which time the beach was adjusted to a 2.65° inclination for Test B4 and then returned to the horizontal.

As previously stated, the results for each experiment have shown themselves to be reproducible within the estimated accuracy of the data. Whenever possible (i.e., whenever the experimental set-up conditions were the same), therefore, the results of set B01 and B02 are compared directly to one another later on.

The results of measurements at both upstream and downstream stations within the surface wind drift layer, in terms of the

relative velocity q, are shown in Figures 7, 8, 9, and 10, each for one of the wind speeds tested. The same effects are observed here as with the B01 data: The drift layer will not admit to a simple Galilean transformation at the speed of the current below. The layer is apparently lagging the current field and relaxing to steady state. The flow combinations of a 2.75 m/sec wind speed and 5.1 cm/sec favorable current, shown in Figure 7, and of a 7.65 m/sec wind speed and a 22.5 cm/sec favorable current, shown in Figure 10, yielded highly distorted drift layer profiles. All of the other conditions tested, however, yielded profiles of the now-familiar drift layer form; that is, monotonically diminishing to zero with depth. The relative velocity q is, of course, dependent upon measurements of the imposed subsurface current field.

Figure 11 shows the distribution of subsurface current along the beach as determined by detailed measurements in the centerline plane for each flow condition tested. Here U_c is the local value of the subsurface current, which was nearly uniform within 4 to 30 cms of depth at a fixed streamwise station. In other words, U_c is the hypothetical 1-D current along the beach. $\overline{U}_c$ is the arithematic average of U_c measured over the length of the beach. It should be noted that the presence of a wind blowing over the water surface had a negligible direct effect on the subsurface current field. The small variation with streamwise position shown in Figure 11 is believed to be caused principally by 3-D structure in the actual recirculating flow.

Proceeding along the lines described above for the B01 data, smooth curves were faired through the data points (except for the two peculiar cases mentioned above), differences formed and relaxation times estimated. Table 3(b) presents the results of these calculations. Here we find evidence, as in Table 3(a) for B01, that τ is constant with depth. Here, again, the results for 4.7 mm depth (and below) must be viewed with an eye towards the previously estimated factor of uncertainty for τ of from $\frac{1}{2}$ to 10. We expect, on physical grounds, that the time constant, describing the relaxation of the upper layers to the perturbing current below, should decrease with depth. The results in Table 3(b) further suggest that the magnitude of τ increases with decreasing wind speed and decreases with favorable current. At a mean depth of 0.71 mm, a wind speed of 4.75 m/sec, and for an adverse current of approximately 8.2 cm/sec, the magnitude of τ is on the order of 200 seconds.

Comparing the results of test B01 to B02 at a wind speed of 6.67 m/sec and an adverse current of (approximately) 9.0 cm/sec, the latter are seen to be larger than the former by a factor of 2 to 3. This variation is, however, well within the range of the expected uncertainty of τ and, in fact, provides a valuable check on the accuracy of the results between separate but, otherwise, identical experiments. Alternately, that data from the two experiments (with identical flow set-up condition) could be taken together to compute a single time constant based on a larger sample size. An examination of the velocity differences for these two tests, given in Table 3(a) and (b), reveals that

this procedure would introduce the full estimated range of uncertainty to the results, in place of the smaller factor when treating the tests separately. The velocity differences are seen in Table 3 to be in agreement with one another within the expected accuracy of $\pm\frac{1}{2}$ cm/sec, which leads to the stated range of uncertainty for τ. This result is not so surprising. It points out that data taken continuously during one experiment shows slightly less variance than data taken over separate experiments (realizations). The stated accuracies of velocity measurements are based on readings taken over many realizations and are accepted as the expected accuracy. For the experiments in question, then, there is nothing to be gained by treating the results together over treating each data set separately for the time constant estimates.

Wave-height temporal frequency spectra were generated from the calibrated output signal of a capacitance wave-height probe utilizing a SAICOR (Model SAI-52B) Real Time Spectrum Analyzer/Digital Integrator. A five-minute long signal record could be processed by utilizing the SAICOR's integrator section. Thirty-two separate spectra are computed, one after the other, while inputting a five-minute long signal record, and frequency averaged by integration to yield a smoothed output spectrum for the full record. The results for only one wind speed will be presented at this time, as being typical, to bring to light some important observations in the data. The remainder of the spectral data and a complete analysis will appear under separate cover in the near future to report the final results and

interpretations of the joint HYDRONAUTICS, Incorporated-Riverside Research Institute 1974 tank tests.

Figures 12 and 13 show spectra measured at stations 3 and 6, respectively, at a constant wind speed of 4.75 m/sec. The vertical scale here is decibels for convenience of interpretation. Note that 10 decibels is equal to 1 decade for power. For clarity of presentation, the spectral plots tagged as 2 and 3 are drawn with their frequency axis shifted horizontally relative to 1 as indicated on the figures. Comparing the results from each figure for the wind-only case, the high-frequency portion of the spectrum centered on the first harmonic of the dominant wave is seen to attenuate with fetch. This is an expected result. At both stations, the effect of a favorable current field, compared to the wind-only case, is to increase the frequency of the dominant wave and to significantly decrease the energy (or amplitude) level of surface wave activity. An adverse current field, on the other hand, decreases the frequency of the dominant wave and only slightly increases the energy level. These effects will be further discussed in Section 4.

3.2.3 Inclined Beach Series - Test B4

Because of considerations of time and completeness, measurements were taken only at station 6 for this beach geometry. We felt that it would be most useful and expedient to put our time and energy for these first tests into a broad range of flow conditions at one station to isolate the discernable effects of wind-wave-current interactions and to consider carefully our ability to quantitatively measure them. Furthermore, the

RRI-TV system, which was plagued with time consuming electronic and microphonic problems that weighed heavily on the program time budget, is not eadily movable.

Figures 14, 15, 16, and 17, each one representing one of the wind speeds tested, present the results of measurements within the drift layer. As for the flat beach data, the measurements are expressed as relative velocity $q = U_D - U_C$, where U_C is the local current speed. The same general trends are evident here as compared to the flat beach case. That is, the (relative) adverse currents are larger than, and the (relative) favorable currents are smaller than the wind-only currents; again, suggesting a phase lag in the response of the drift layer to perturbations in the subsurface current field.

Smooth curves have been faired through the data points for the two lower wind speeds, shown in Figures 14 and 15. The results for the higher wind speeds (Figures 16 and 17) and favorable currents are not so easily described in that the data points are scattered and cannot be connected by a simple curve. In all cases the data were reproducible. Therefore, the qualitative differences between the results at different wind speeds are viewed as real distortions in the mean flow field that are time-independent. Measurements of the local subsurface current speed were also taken for each test set-up in order to construct the relative velocity q.

Figure 18 is a plot of the experimental subsurface current speeds measured along the length of the beach in the longitudinal plane of the centerline. Comparing the measurements to

the theoretical 1-D result (representing a hyperbolic variation of current with local water depth) in Figure 18, it is clear that the experimental flow was rather more complex. The effect of three-dimensionality of the current field on the drift measurements is unknown at this time. As previously discussed, the issue was avoided as far as possible by limiting the range of current speed to minimize 3-D distortions.

Wave height-temporal frequency spectra, for a wind speed of 4.75 m/sec in combination with favorable, adverse, and zero current fields on the inclined beach, are presented in Figure 19. Here, again, the spectral plots have been horizontally shifted relative to one another for clarity. Comparing the results for the wind-only case in Figure 19 (for an inclined beach) to those in Figure 13 (for a flat beach) at the same wind speed and fetch, we find agreement. Increasing favorable current results in a higher dominant wave frequency and in a strikingly lower spectral energy level. Increasing adverse current yields a lower dominant wave frequency and only a very slightly higher spectral energy level. Another effect, that is not so obvious in Figure 19 in which all three spectra are plotted on the same scale to highlight relative differences in the high energy portions, is that an adverse current increases, and a favorable current decreases, the relative wave energy in the high frequency portion of the spectrum in the vicinity of the first harmonic of the dominant wave. This point is illustrated in Figure 20. The spectrum for the adverse current run (curve 1, Figure 19) and for the favorable current run (curve 3, Figure 19) are scaled to yield the best comparison of relative energy

levels and plotted together in Figure 20. The adverse current run is seen to have a dominant temporal frequency of 3.08 cps and a clearly discernible first harmonic. The favorable current run, on the other hand, has a dominant frequency of 4.51 cps and a barely perceptible first harmonic. The fetch is effectively reduced by the favorable current and increased by the adverse current, compared to the wind-only case. In section 3.2.2, the effect of fetch was shown to reduce the energy of the harmonic. Therefore, the spectrual modification noted above is felt to be due to current rather than to fetch.

4. DISCUSSION

There are three important aspects of the experiment to be further discussed in this section; namely, wind-wave generation, mean recirculating flow-establishment and characteristics, measurements of wind-drift layer distortions and surface wave spectra modulations. The latter is, of course, the most relevant here. However, to establish the highest level of confidence in the experimental results, our aim is to describe the test conditions and to present the details of the measurements as completely and as accurately as possible.

4.1 Wind-Wave Generation

The wind-wave tank has been utilized over the past several years in studies directly related to the present one. We have attempted to draw from the large body of calibration data and operating characteristics in existence for the facility whenever appropriate and possible. Previous studies differ from the present one in at least two important respects. In the present

case, measurements were taken at several downwind stations, while in the past, attention was normally concentrated at one station or at least over only a small downwind interval. The present results include the effects of wind and of current, while previous studies generally include that of the wind alone. Figure 3 presents the wave-characteristics of the water surface as a function of wind speed for the wind-only case, for both the previous and the present studies. Similarly, measurements of the wind-induced surface drift current have been presented in Figure 4. The important points to note here are that while the agreement between the previous and the present data are fairly good there is a discernible, but small, fetch effect due to the downwind evolution of the surface wave spectrum and the wind profile. We treated the results as being essentially independent of this effect by comparing (at each station) the data for the cases with non-zero current to that for the wind-only. In other words, we treated the wind-only data at each station as a "tare" measurement and were able thereby to proceed further with the data to estimate the relaxation time constants as previously described.

The results for the two lower wind speeds and corresponding current fields have been given for the flow over a flat beach in Figures 7 and 8 and for the flow over an inclined beach in Figures 14 and 15. Examination of the data in each of the figures, comparing the wind-only case to that for both favorable and for adverse current, it appears that the slopes $\partial q/\partial Z$, in the linear region near to the water surface, are the same. In other words,

indications are that for the lower values of wind speed and currents tests, the friction velocity, $w_* = \nu_w (\partial q_{(o)}/\partial Z)^{\frac{1}{2}}$, where ν_w is the kinematic viscosity of the water, is a direct function of wind speed only and, thereby, also a weak function of fetch. This is not so for the higher wind speeds and currents tested, as indicated in Figures 5, 9, and 10 for the flat beach, and Figures 16 and 17 for the inclined beach. For these cases, the slopes of the drift profiles at a given wind speed apparently vary with the imposed current field: We expect, on kinematic grounds at least, that the shear velocity will be increased by the presence of an adverse current field and decreased by a favorable one. These results suggest that the modification of friction velocity by a subsurface velocity is a second-order effect of the ratio of wind-induced surface drift to current speed and remains small except as the ratio becomes unity or larger. Data are not yet available to resolve this point; direct measurement of the shear stresses may be necessary.

In summary, then, the wind and surface wave characteristics measured in this study agree fairly well with those of previous studies. There is a discernible effect of fetch on the results at different measuring stations. The shear velocity is seen to be decreasing downwind. Taking the surface drift currents measured at upstream and downstream stations to Figures 2 and 4, we can estimate, for the wind-only case, the local wind speed and, thereby, the magnitude of the shear velocity at each station. Between stations 2 and 6, the changes in shear velocity inferred in this manner are on the order of 10 percent/meter.

The presence of a subsurface current field apparently has an effect on the magnitude of the shear velocity which becomes more pronounced as the ratio of wind-induced surface drift to current speed increases. This effect is, however, not yet understood.

4.2 Mean Recirculating Flow - Establishment and Characteristics

The submerged, stationary beach-recirculating current system is an essential part of these experiments in that it provides subsurface currents and current gradients to simulate important features of progressive internal waves in a laboratory facility of limited size. The present configuration has been shown to be incapable of producing uniform, mean current fields over a large speed range. This problem can and will soon, no doubt, be resolved with the addition to the system of properly designed diffusing and smoothing sections. In order that this source of unwanted flow distortions may not become a rug under which all difficulties (including, perhaps, some subtle aspects of the physics) and unexplainable data be swept, it is appropriate that we discuss it further with all the facts in hand.

Meandering of the floats from their drop-points along the tank centerline to either side wall gave the first indication of non-parallel current flow. Float size, beach orientation, fetch, as well as wind speed and current were all important parameters. Sometimes a float would travel along the centerline for a meter or more and then suddenly veer to the side. Once a float left the centerline and moved to one side or the other, it remained there as it was carried downwind. We investigated the structure of the current field visually by means of vegetable dyes and

were thus able to discern the presence of longitudinal vorticity within the current field. The strength of this vorticity, as indicated by the rotational velocity of the dyed fluid and the coherence of its 3-D structure, varied with the speed of the current (i.e., impeller RPM) and the orientation of the beach to the current. Based on dye observations and consideration of the vorticity theorems of basic fluid mechanics, we feel that the vorticity we saw is, for the most part, the natural outcome of the geometry of the recirculating flow over the beach and of the impeller which drives the flow. Both of these effects can, of course, be greatly attenuated if not eliminated, with proper smoothing and straightening of the flow.

An additional source of vorticity and three-dimensionality, not yet discussed, results from the flow geometry for the case of adverse currents in the wind-wave-current facility. Referring to Figure 21, the drift profile for the case of adverse currents must have a zero crossing to match the wind-induced drift layer to the current field below. Stagnation points would, then, exist at the surface somewhere both upstream and downstream. It is obviously impossible to maintain the "bubble" shown and satisfy a two-dimensional mass balance. The flow field must be three-dimensional someplace, at least near the stagnation points. This three-dimensionality is a form of vorticity.

In general, distortions to the mean flow were found to be small, and the occurrence of veering floats, infrequent, for both adverse and favorable currents $\lesssim 15$ cm/sec. Put in more quantitative terms; for currents $\lesssim 15$ cm/sec, it was difficult

to perceive any 3-D vertical structure in the dyed (turbulent) flow field, and we could expect on the average of one float in 10 to veer. By comparison, for currents in excess of 20 cm/sec, we could expect as many as 5 out of 10 floats to veer. The distortions, shown in Figures 10, 16, and 17, are believed to be the result of the presence of strong longitudinal vorticity in the current field.

Flow separation from the beach support struts at the side walls of the tank were also troublesome. These were, however, more of a problem at the lower current speeds (and corresponding wind speeds); first of all, because the surface wave activity and the turbulence level in the water were less, enabling a longer life, and second of all, because they could more readily move away from the wall toward the center of the tank where the drift measurements were taken. The distorted drift profile, shown in Figure 7 for a favorable current of 5.1 cm/sec, is believed to be the result of vertical vorticity shed from the beach support struts. The solution to this problem would be simply to redesign the beach and support it from below.

4.3 Measurements

4.3.1 Wind Drift Layer Distortions

The results of our measurements indicate that changes in the structure of the wind-induced drift layer produced by the simulated internal wave current field in these experiments are discernible and measurable, though quantitatively quite small. It is the interpretation of such measurements that makes

them difficult and not the actual data taking which is an objective process. As previously discussed, the preliminary experiments to optimize the data-taking scheme for minimum standard deviation have proven to be very helpful in this regard. The data bars, shown in Figure 5, that are believed to be appropriate for all the measurements, are the outcome of this preliminary study. Moreover, the smoothness and self-consistency of the data--with exception of those distortions particular to the background mean flow as discussed above--tend to increase our confidence in the results as tabulated in Tables 3(a) and 3(b). The same qualitative results were obtained for all flow conditions tested and for both the flat and the inclined beach configurations; that is, the relative velocity in the presence of an adverse current field was always greater than, and in the presence of a favorable current field was always smaller than that for the wind alone. These differences apparently decrease in the downwind direction. In other words, some time is required for the drift layer to adjust itself to changes in the velocity of the fluid below.

An explanation for the smallness of the measured changes in the drift layer can be seen from the results in Tables 3(a) and 3(b). The actual travel time between measuring stations at a given mean depth below the surface is estimated by $\Delta x/\overline{U}_{avg}$. Comparing these values to those for the estimated relaxation time τ, we see that travel times were typically only 10 to 20 percent of the relaxation times. This is, of course, another way of saying that the distance between the

measuring stations was small compared to the relaxation length scale. These results also suggest that for a constant wind speed, the ratio of τ for an adverse current of (approximately) 9 cm/sec to τ for a favorable current of the same magnitude is (approximately) 2. However, this ratio for an adverse current of 9 cm/sec and a favorable current of 23 cm/sec jumps to (approximately) 10.

There is insufficient information at this time to permit parameterization of the flow processes. Still, certain trends pointed out in Section 3.2 are evident and worth mentioning here again: Relaxation times are seen to be nearly constant with mean depth, to decrease with wind speed, to increase with adverse current speed, and to decrease with favorable current speed. Also, the effects of current gradient cannot yet be assessed and await further tests.

4.3.2 Surface Wave Spectra Modulations

Awaiting the RRI report on their measurements of the wave slope spectra for the flow conditions reported here, only preliminary remarks can be made at this time based on our wave height data. Figures 12 and 13 for the flat beach tests (B02) and Figures 19 and 20 for the inclined beach tests (B4) have already been presented as typical. A line drawn on the figures at a slope of -5 provides for comparison of the high frequency portion of the spectrum in the wave-wind facility to that predicted by Phillips[12] for the case of infinite fetch. A recent calibration of wave-height probe frequency response shows a fall-off of -20Db per decade from a frequency of 4 to 8

cps. Correcting the spectra already presented for this effect results in fairly good agreement with Phillips' (-5) prediction in the high frequency portion of the spectrum. Corrected spectra are not shown here but will be presented in detail in the aforementioned final report of the HYDRONAUTICS, Incorporated-Riverside Research Institute 1974 tests.

The spectra measured in the limited fetch, wind-wave tank relative to Phillips' (-5) spectrum are over-driven at the frequency of the dominant wave, exhibit a second peak in the vicinity of the first harmonic of the dominant wave frequency and fall into agreement only for frequencies above (approximately) 7 cps.

There are several effects brought to light by this data. The results in Figure 12 show that as the current is increased in the favorable sense, the spectrum energy level decreases significantly, here by an order of magnitude. This could perhaps be the result of a reduced shear velocity produced by a relaxing surface when the current is in the direction of the wind. The adverse current does not, however, produce the opposite effect. The principal effect of an adverse current has been shown in Figure 20 to be an increase in the spectrum energy only in the vicinity of the harmonic of the dominant wave. These results taken together suggest the effect to be rather of fetch (or time) in that the spectrum has more time to develop in the case of an adverse current, owing to the correspondingly smaller mean convective speeds. Comparing the results in Figure 13 for the flat beach to those in Figure 19 for the inclined

beach, at the same wind speed and very nearly the same local currents, the spectrum energy reduction due to a favorable current is significantly larger for the inclined than for the flat beach. This suggests one possible effect of local current gradient.

5. CONCLUDING REMARKS

An understanding of the individual and combined effects of wind speed, current speed and direction, current gradient and fetch (or time) in wind-wave-current interactions is of obvious and immediate importance. The emphasis in the first experiments has been rather diffused over all of the parameters in order to gain some insight into their relative importance for more effective subsequent experimental attacks. In spite of the hinderances imposed by a mean flow suffering from unwanted 3-D distortions, the results of the present experiments provide clear evidence of the character of the interaction phenomenon as well as useful information on the trends produced by variations of both wind speed and current. The important effects, distortions and trends observed in these first experiments have been described and briefly discussed. Much more data is needed, however, before a clear picture of the processes involved and the roles of each of the parameters can be brought to the front.

We expect that the effects of wind speed and current will be correlated with the speed ratio $U_{D_o}/U_{c\ max}$. To minimize mean flow distortions due to sources other than direct wind-wave-current interactions, the values of U_{D_o} and $U_{c\ max}$ must be

judiciously chosen. Recall that theoretical considerations suggest a speed ratio (absolute value) in the vicinity of unity for maximum interaction effects. Small speeds, on the one hand, can produce conditions where the effects of interactions are also small and difficult to perceive; while large speeds, on the other, can produce conditions where travel, and hence, interaction times are short in a length-limited facility. Future experiments performed at a moderate wind speed, say, 4.75 m/sec, with values of current selected for a broad range of speed ratio, would provide data to elucidate the role of the speed ratio.

It is, no doubt, significant that over the range of conditions tested, the distortions within the drift layer, supposedly produced by the presence of the current field, and the corresponding modulations of the surface wave spectra could no where be called other than very small. These observations will be cast into more quantitative measure when the RRI results become available. Distortions within the drift layer have been measured. The corresponding temporal frequency spectra results presented here, however, show no striking modulations, either narrow or wide band.

Before the laboratory results can be applied to conditions encountered in the field, the appropriate scaling laws must first be determined. How to compare the laboratory drift layer to a typical oceanic drift layer? How to compare the effective internal wave period and wavelength in the laboratory to those for a typical oceanic internal wave? How to compare the measured

results for a stationary beach to those for a progressive internal wave? These questions are presently under theoretical consideration, while the findings and results of the experimental tests are being carefully analyzed and applied to the design of a modified facility and the next test program.

REFERENCES

1. Phillips, O. M., "Surface Wave Effects Produced by Internal Waves," HYDRONAUTICS, Incorporated Technical Report 7015-3, October 1971.

2. Phillips, O. M., "The Influence of Wind Drift and Capillarity on Blockage," HYDRONAUTICS, Incorporated Technical Report 7211-1, May 1973.

3. Phillips, O. M., "Surface Effects--An Analysis and Review of Processes Involved and Phenomena Observed," HYDRONAUTICS, Incorporated Technical Report 7211-9, December 1974.

4. Vaglio-Laurin, R., "Discussion at ARPA Meeting, May 30, 1973.

5. Lighthill, M. J., "The Response of Laminar Skin Friction and Heat Transfer to Fluctuations in the Stream Velocity," Proc. Roy. Soc., Ser. A, Vol. 224, pp. 1-23, 1954.

6. Reynolds, W. C., and Hussain, A. K. M. F., "The Mechanics of an Organized Wave in Turbulent Shear Flow. Part 3. Theoretical Models and Comparisons with Experiments," JFM, Vol. 54, pp. 263-289, 1972.

7. Phillips, O. M., and Banner, M. L., "Wave Breaking in the Presence of Wind Drift and Swell," JRM, Vol. 66, pp. 625-640, 1974.

8. Lewis, J. E., Lake, B. M., and Ko, R. S., "On the Interaction of Internal Waves and Surface Gravity Waves," JFM, Vol. 63, pp. 773-800, 1974.

9. King, M., and Lizzi, F., "A Television System for the Real-Time Spectrum Analysis of Ocean Waves," Riverside Research Institute Technical Report No. PTP-91, 13 September 1972.

10. Wu, J., "Laboratory Studies of Wind-Wave Interactions," HYDRONAUTICS, Incorporated Technical Report No. 231-13, June 1967.

11. Wu, J., "Wind-Induced Drift Currents," HYDRONAUTICS, Incorporated Technical Report 7303-3, August 1973.

12. Phillips, O. M., "The Equilibrium Range in the Spectrum of Wind Generated Waves," JFM, Vol. 4, pp. 426-434, 1958.

Table 1. Preliminary Float-Drift Current Measurements

Mean Depth, mm	Current U_c = 0 (cm/sec)						U_c = + 9.2						U_c = - 9.3					
	Station 1-3			Station 5-7			Station 1-3			Station 5-7			Station 1 - 3			Station 5 - 7		
	Trials	$\bar{U}_D$	σ	Trials	$\bar{U}_D$	σ	Trials	$\bar{U}_D$	σ	Trials	$\bar{U}_D$	σ	Trials	$\bar{U}_D$	σ	Trials	$\bar{U}_D$	σ
0.71	120	19.31	.56	60	17.50	.35	10	25.03	-	20	25.16	.53	20	13.05	.49	20	10.19	.56
1.19	30	18.90	.60	30	16.23	.75	20	23.33	.46	20	23.95	.09	60	9.54	.42	20	8.44	.40
2.37	20	15.52	.38	30	14.82	.64	30	19.61	.34	20	20.05	.55	60	8.33	.44	20	5.32	.04
4.22	20	12.40	.30	30	12.44	.38	20	19.09	.14	20	18.74	.45	50	5.10	.24	20	4.67	.13
25.40	15	6.23	.03	30	6.43	.03	20	13.77	.06	20	13.12	.07	-	-	-	-	-	-

Wind Speed U_W = 6.7 M/sec.

Station 1 - 3 = 121.6 cms

Station 5 - 7 = 121.9 cms

$$\sigma^2 = \frac{\Sigma_i X_i^2 - N\bar{X}^2}{N}$$

Table 2a

Data Set B01

ARPA WIND-WAVE-CURRENT INTERACTION EXPERIMENT TEST MATRIX

BEACH ANGLE	h_o (cm)	U_{cmx} (cm/s)	U_W (m/s)	U_{D_o} (cm/s)	$\frac{U_{D_o}}{U_{cmx}}$	U_{cmn} (cm/s)	MEASURE STATIONS	MEASURE DEPTHS (mm)
0°	68.7	0	6.67	22.00	-	0	1-3	B01-C0-W3-S0
		0		19.00	-	0	5-7	B01-C0-W3-S1
		9.30		22.00	2.37	9.30	1-3	B01-C20-W3-S0
		9.30		19.00	2.04	9.30	5-7	B01-C20-W3-S2
		-9.20		22.00	-2.39	-9.20	1-3	B01-C60-W3-S0
		-9.20		19.00	-2.06	-9.20	5-7	B01-C60-W3-S2

Table 2b

Data Set B02

ARPA WIND-WAVE-CURRENT INTERACTION EXPERIMENT TEST MATRIX

BEACH ANGLE	h_o (cm)	U_{cmx} (cm/s)	U_W (m/s)	U_{D_o} (cm/s)	$\frac{U_{D_o}}{U_{cmx}}$	U_{cmn} (cm/s)	MEASURE STATIONS	DATA CODE NO.
0°	68.7	5.10	2.85	9.0	1.76	5.10	2-4	B02-C10-W1-S1-1111
		5.10	2.85	9.20	1.80	5.10	5-7	B02-C10-W1-S2-1021
		9.50	2.85	9.0	.95	9.50	2-4	B02-C20-W1-S1-1111
		8.90	2.85	9.20	1.03	8.90	5-7	B02-C20-W1-S2-1101
		9.20	4.75	15.50	1.68	9.20	2-4	B02-C20-W2-S1-1112
		8.60	4.75	16.40	1.91	8.60	5-7	B02-C20-W2-S2-1101
		24.20	6.67	22.00	.91	24.20	2-4	B02-C40-W3-S1-1113
		22.01	6.67	23.50	1.07	22.01	5-7	B02-C40-W3-S2-1104
		23.25	7.65	28.50	1.23	23.25	2-4	B02-C40-W4-S1-1114
		21.70	7.65	29.50	1.36	21.70	5-7	B02-C40-W4-S2-1024
		-5.15	2.85	9.0	-1.75	-5.15	2-4	B02-C60-W1-S1-1114
		-5.15	2.85	9.20	-1.79	-5.15	5-7	B02-C60-W1-S2-1025
		-8.48	4.75	15.50	-1.83	-8.48	2-4	B02-C80-W2-S1-1030
		-7.90	4.75	16.40	-2.08	-7.90	5-7	B02-C80-W2-S2-1118
		-8.80	6.67	22.00	-2.50	-8.80	2-4	B02-C80-W3-S1-1031
		-8.36	6.67	23.50	-2.81	-8.36	5-7	B02-C80-W3-S2-1119

TABLE 2c - ARPA WIND-WAVE-CURRENT INTERACTION EXPERIMENT TEST MATRIX DATA SET B4

BEACH ANGLE	h_o (cm)	U_{cmx} (cm/s)	U_W (m/s)	U_{D_o} (cm/s)	$\frac{U_{D_o}}{U_{cmx}}$	U_{cmn} (cm/s)	$U_{c@⑥}$ (cm/s)	$\frac{1}{Uc}\frac{dU_c}{dx}\Big\|_{@⑥}$	T (min/cyc) @⑥	MEASURE STATIONS	DATA CODE NO.
2.65°	54.00	7.20	2.85	9.20	1.28	4.32	5.65	8.06×10^{-4}	18.20	(5 - 7)	B4-C1-W1-S2-1008
		13.20	4.75	16.80	1.27	7.92	11.15	5.38×10^{-4}	14.75		B4-C2-W2-S2-1009
		15.90	6.67	24.60	1.55	9.54	13.91	4.72×10^{-4}	14.85		B4-C3-W3-S2-1010
		22.20	6.67	24.60	1.11	13.32	18.20	6.13×10^{-4}	7.70		B4-C4-W3-S2-1009
		22.20	7.65	29.00	1.31	13.32	18.20	6.13×10^{-4}	7.70		B4-C4-W4-S2-1011
		-5.85	2.85	9.20	-1.57	-3.51	-4.80	5.47×10^{-4}	32.50		B4-C6-W1-S2-0926
		-10.45	4.75	16.80	-1.61	-6.27	-8.50	6.12×10^{-4}	16.36		B4-C7-W2-S2-0926
		-10.45	6.67	24.60	-2.35	-6.27	-8.50	6.12×10^{-4}	16.36		B4-C7-W3-S2-0930
		-13.20	6.67	24.60	-1.86	-7.92	-11.40	4.70×10^{-4}	16.82		B4-C8-W3-S2-1003
		-13.20	7.65	29.00	-2.20	-7.92	-11.40	4.70×10^{-4}	16.82		B4-C8-W4-S2-1004
		CALIBRATION RUNS - WIND ONLY									
		0	2.85	9.20							B4-C0-W1-S2-0919
			4.75	16.80							B4-C0-W2-S2-0920
			6.67	24.60							B4-C0-S3-S2-0920
			7.65	29.00							B4-C0-W4-S2-0920

Table 3a

Estimates of Relaxation Time Constants

(Data Set B01, Flat Beach)

Wind Speed = 6.67 m/sec

	ADVERSE CURRENT ≅ -9.3 cm/sec					FAVORABLE CURRENT ≅ +9.2 cm/sec				
Mean Depth, mm	$(q-q_o)_{1-3}$	$(q-q_o)_{5-7}$	$\bar{U}_{avg.}$	$\frac{\Delta X}{\bar{U}_{avg.}}$	τ(sec)	$(q-q_o)_{1-3}$	$(q-q_o)_{5-7}$	$\bar{U}_{avg.}$	$\frac{\Delta X}{\bar{U}_{avg.}}$	τ(sec)
0.71	2.94	1.90	11.62	20.96	48	-2.50	-1.57	25.10	9.71	21
1.19	2.30	1.59	10.02	24.31	66	-3.00	-1.73	24.34	10.00	18
2.37	2.01	1.40	7.51	32.48	90	-4.12	-2.50	20.93	11.54	23
4.72	1.89	1.52	4.93	49.40	227	-3.40	-2.44	19.41	12.55	38

Table 3b

Estimates of Relaxation Time Constants

(Data Set B02, Flat Beach)

Wind Speed = 6.67 m/sec

	ADVERSE CURRENT ≃ -8.60 cm/sec					FAVORABLE CURRENT ≃ 22.60 cm/sec				
Mean Depth, mm	$(q-q_o)_{2-4}$	$(q-q_o)_{5-7}$	$\bar{U}_{avg.}$	$\frac{\Delta X}{\bar{U}_{avg.}}$	τ (sec)	$(q-q_o)_{2-4}$	$(q-q_o)_{5-7}$	$\bar{U}_{avg.}$	$\frac{\Delta X}{\bar{U}_{avg.}}$	τ (sec)
0.71	2.35	2.15	13.60	13.17	148	3.1	2.0	40.00	4.48	10
1.19	2.15	1.95	11.86	15.10	155	2.85	2.1	38.74	4.62	15
2.37	2.0	1.80	8.84	20.25	192	2.3	2.0	35.64	5.02	36
4.72	1.8	1.70	5.74	31.19	545	1.9	1.7	32.95	5.43	49

continued -

Table 3b - continued

Wind Speed = 4.75 m/sec

	ADVERSE CURRENT ≅ - 8.20 cm/sec					FAVORABLE CURRENT ≅ 8.90 cm/sec				
Mean Depth, mm	$(q-q_o)_{2-4}$	$(q-q_o)_{5-7}$	$\bar{U}_{avg.}$	$\frac{\Delta X}{\bar{U}_{avg.}}$	τ(sec)	$(q-q_o)_{2-4}$	$(q-q_o)_{5-7}$	$\bar{U}_{avg.}$	$\frac{\Delta X}{\bar{U}_{avg.}}$	τ(sec)
0.71	1.80	1.60	7.72	23.20	200	2.3	2.4	20.80	8.61	-
1.19	1.70	1.45	6.74	26.60	170	2.2	2.0	20.10	8.91	94
2.37	1.90	1.60	4.83	37.30	217	2.05	1.80	18.40	9.73	75
4.72	1.75	1.50	3.33	53.77	350	2.0	1.80	17.10	10.47	100

continued -

Table 3b - concluded

Wind Speed = 2.85 m/sec

	FAVORABLE CURRENT ≅ 9.2 cm/sec				
Mean Depth, mm	$(q-q_o)_{2-4}$	$(q-q_o)_{5-7}$	$\overline{U}_{avg.}$	$\frac{\Delta X}{\overline{U}_{avg.}}$	τ (sec)
0.71	2.35	2.25	15.60	11.48	264
1.19	2.40	2.30	15.10	11.86	280
2.37	2.40	2.25	14.40	12.43	200
4.72	2.60	2.25	13.40	13.36	96

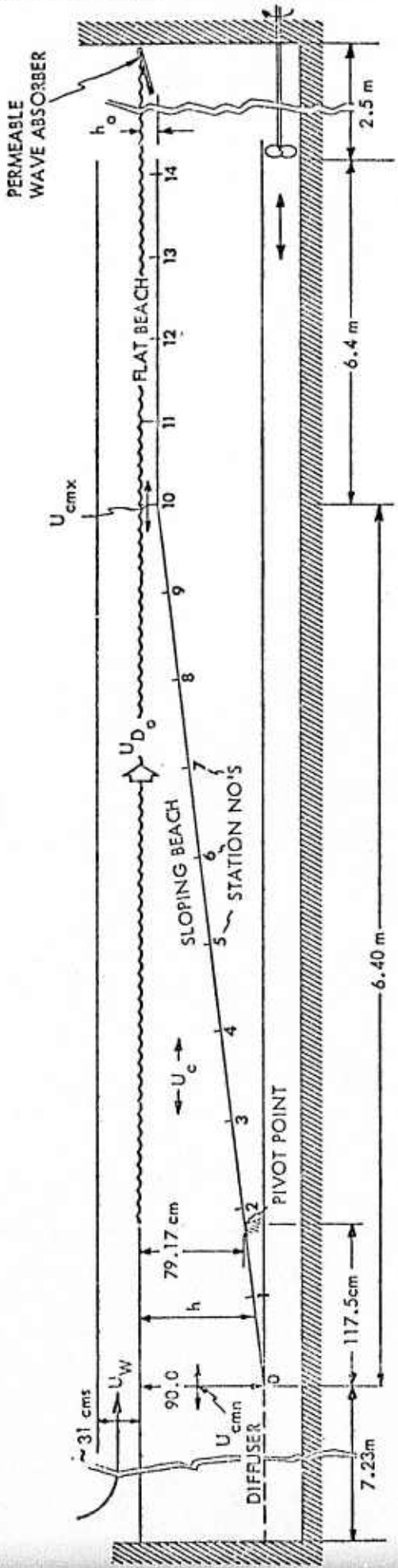

FIGURE 1 - SCHEMATIC OF WIND-WAVE-CURRENT FACILITY
(SHOWING SUBMERGED BEACH AND CURRENT
GENERATION SYSTEM)

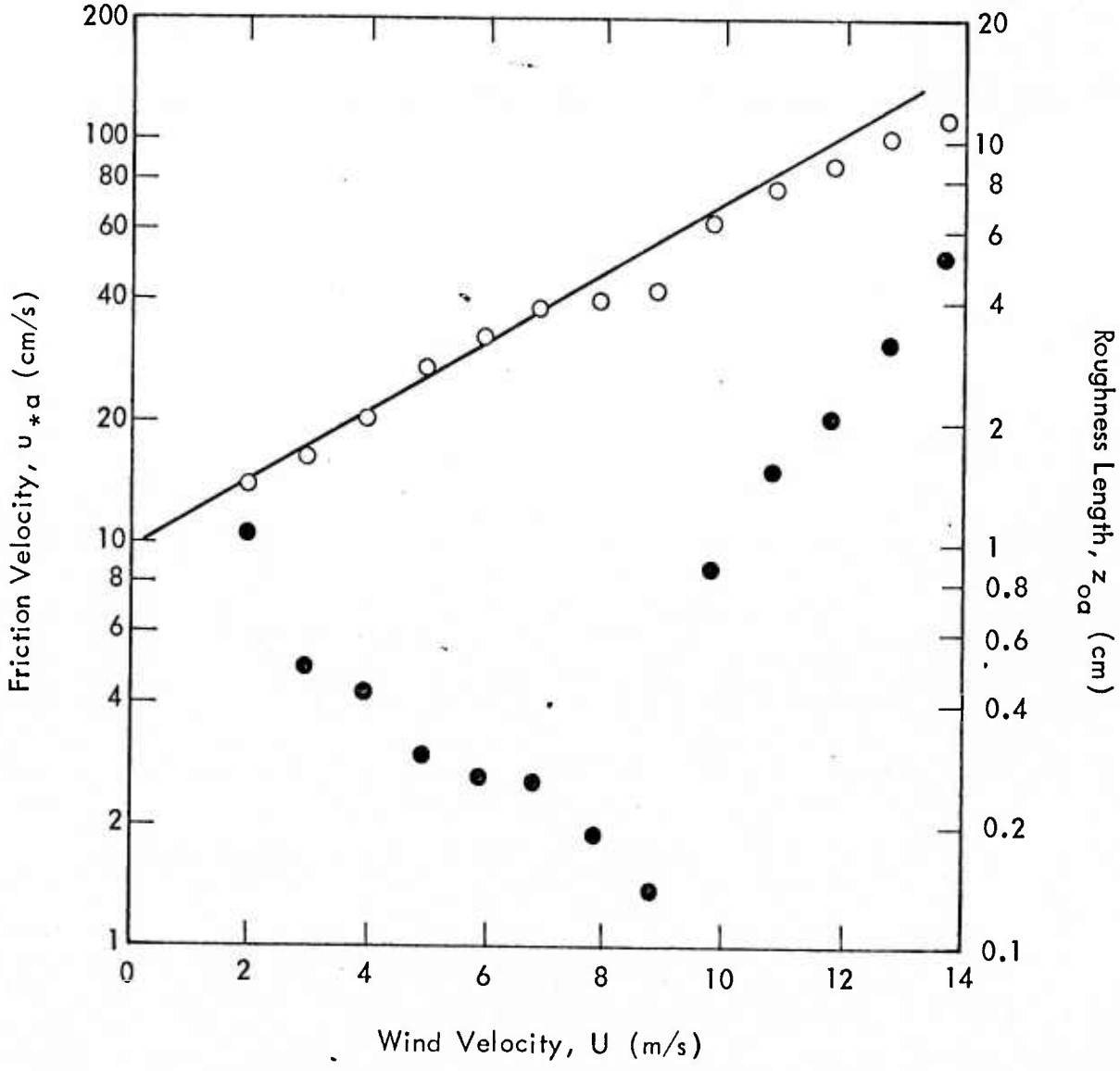

FIGURE 2 - FRICTION VELOCITY OF WIND AND ROUGHNESS LENGTH OF WIND BOUNDARY LAYER. The open circles indicate the friction velocity and the solid circles indicate the roughness length.

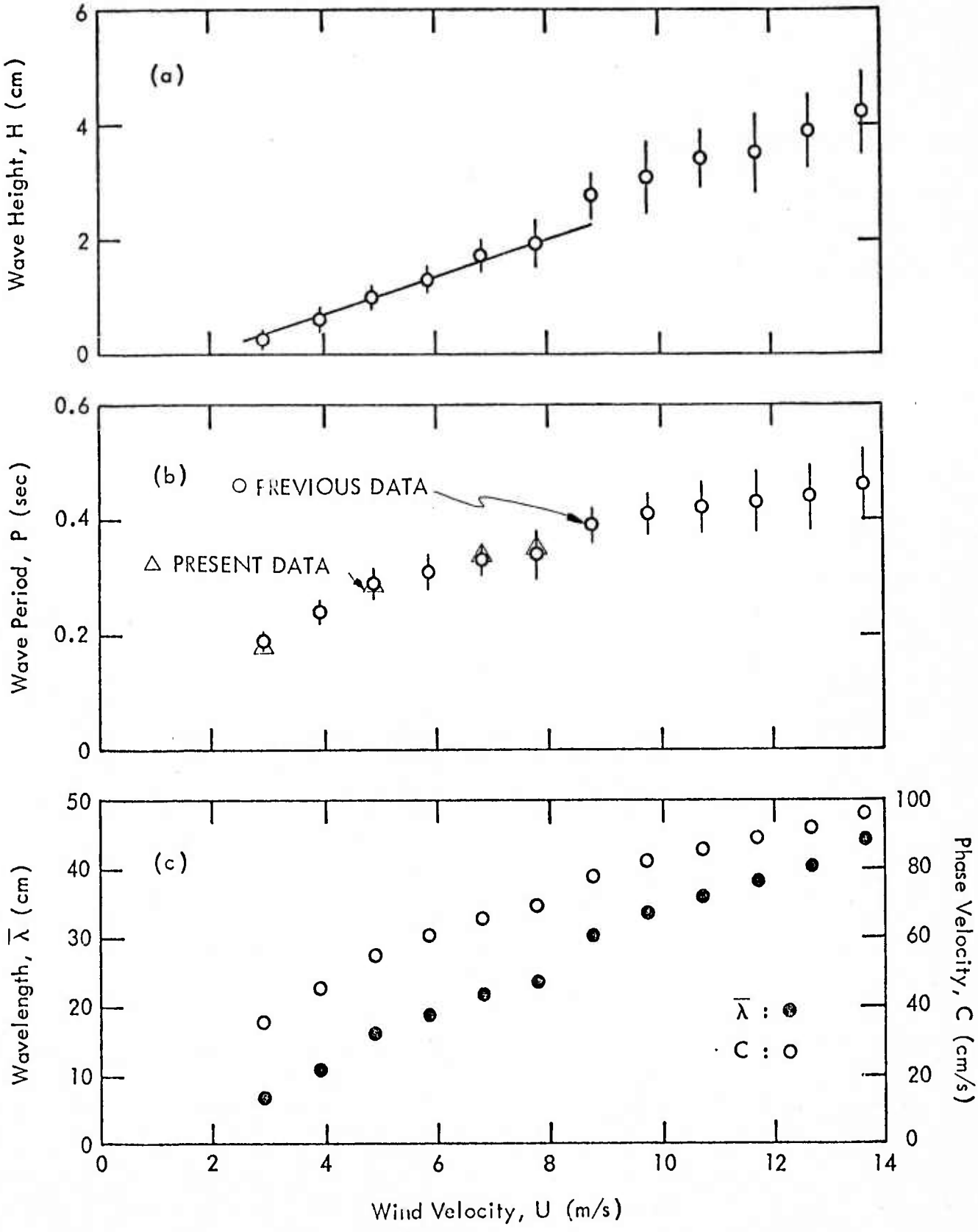

FIGURE 3 - WAVE HEIGHTS, WAVE PERIODS, WAVELENGTHS, AND PHASE VELOCITIES UNDER VARIOUS WIND VELOCITIES

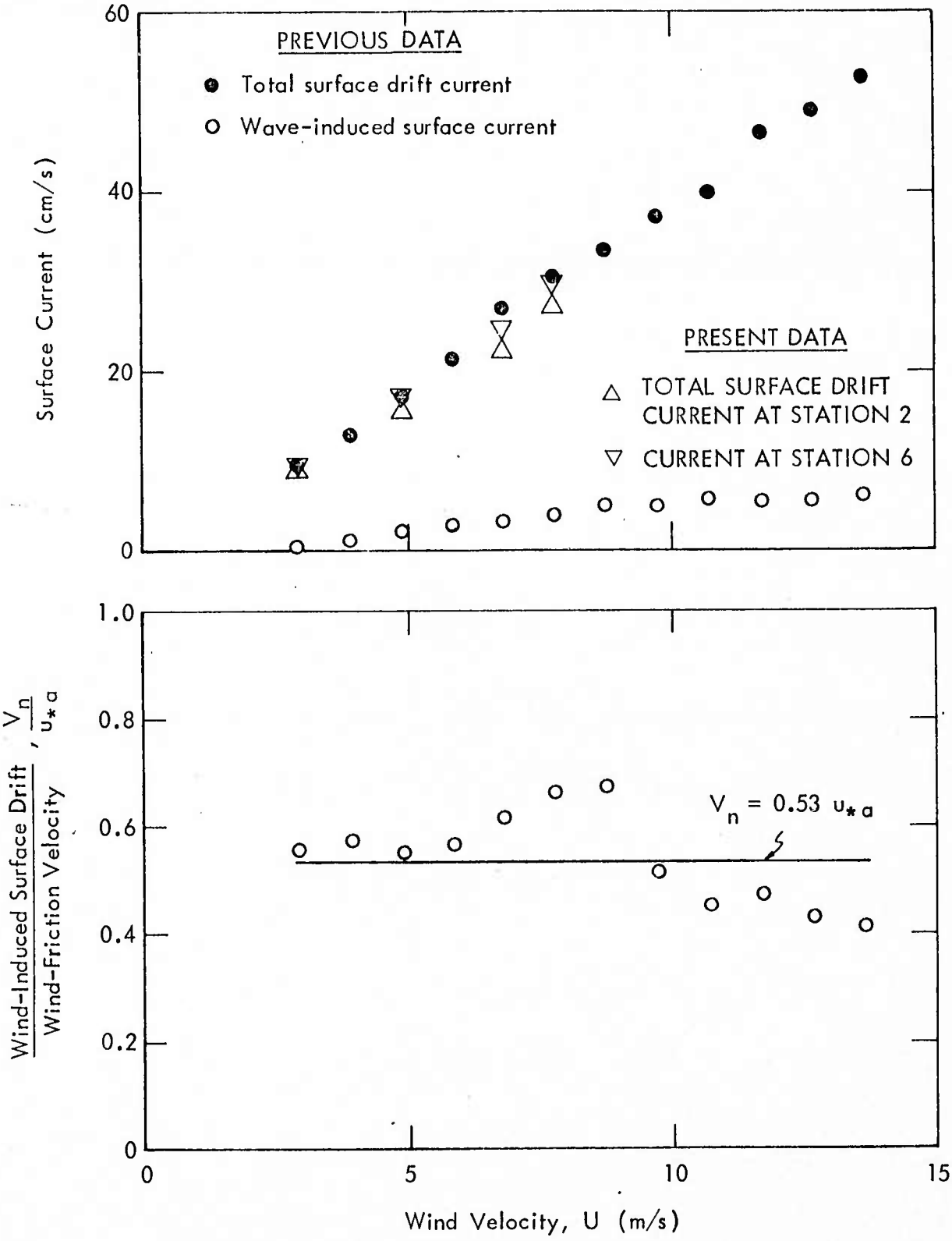

FIGURE 4 - WIND-INDUCED AND WAVE-INDUCED SURFACE CURRENTS UNDER VARIOUS WIND VELOCITIES

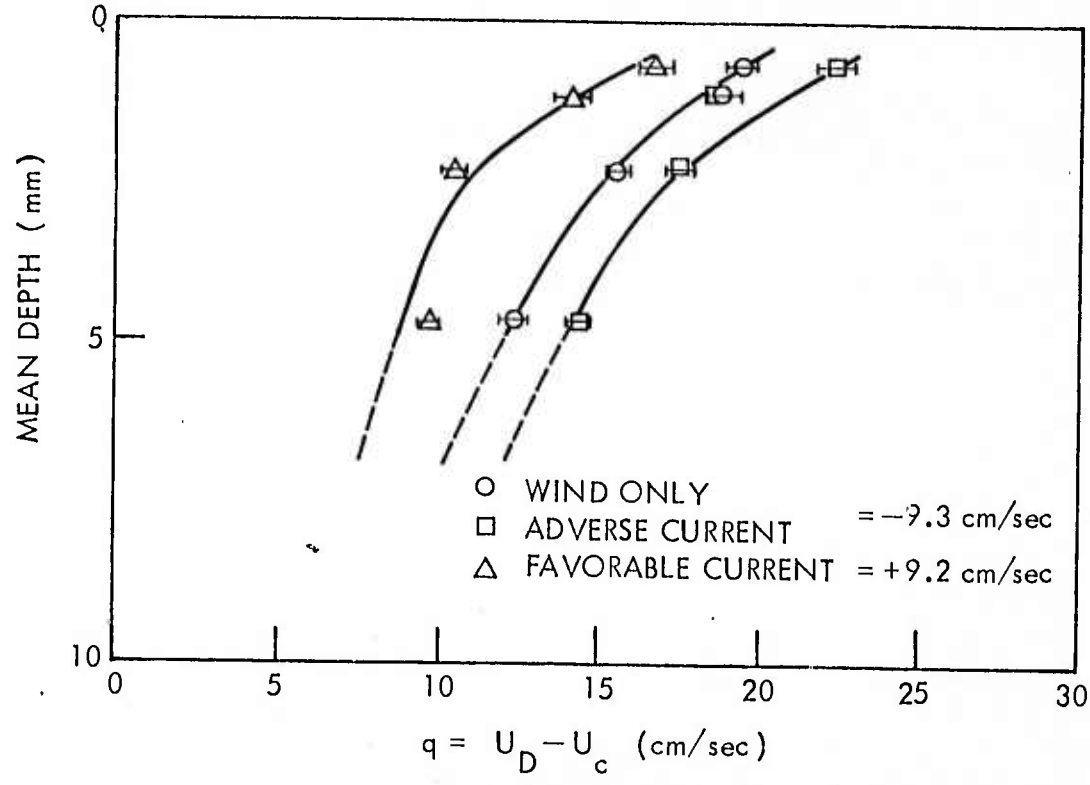

(a) STATIONS 1 - 3

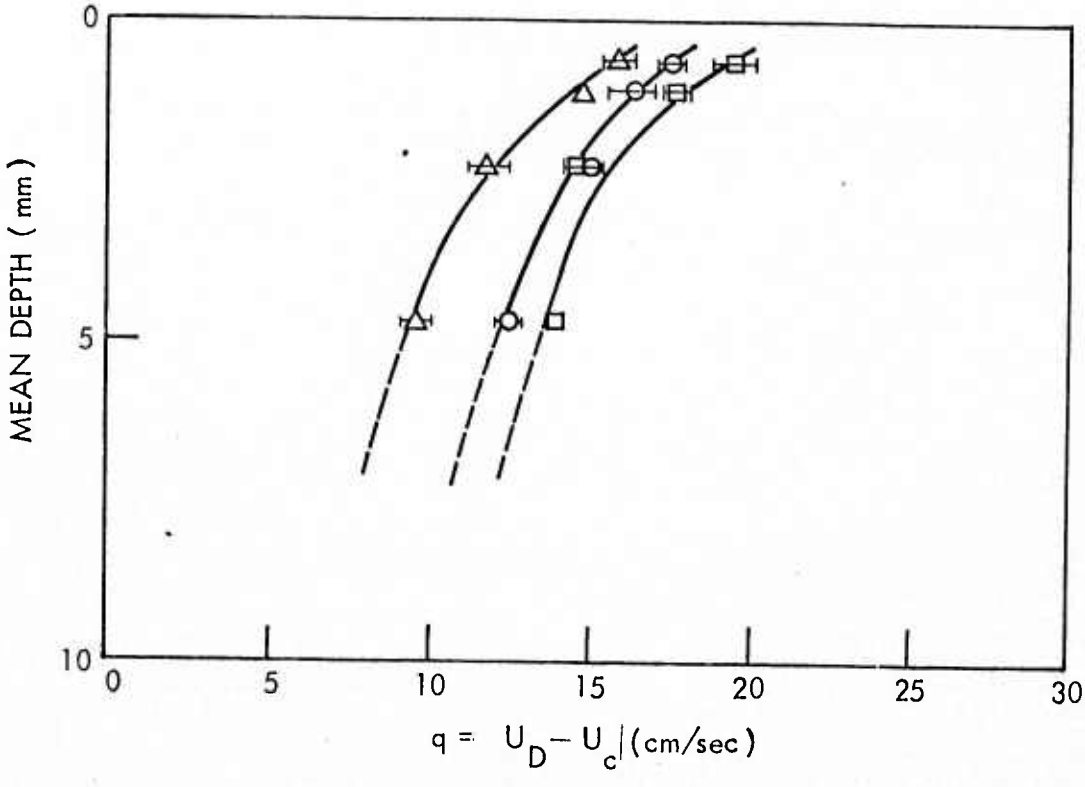

(b) STATIONS 5 - 7

FIGURE 5 - DRIFT CURRENT VS. DEPTH (Data Set B01, Flat Beach)

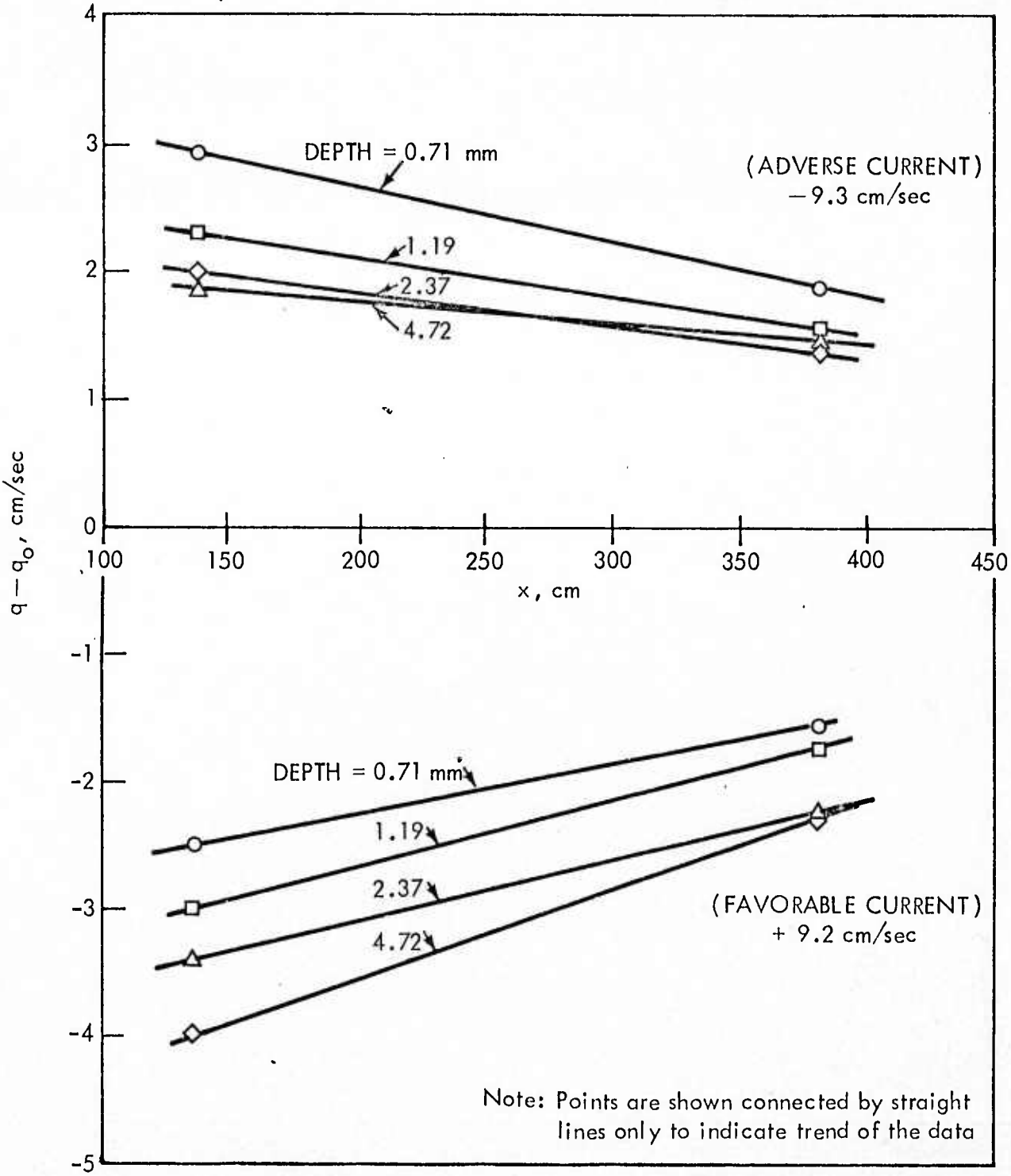

FIGURE 6 - RELATIVE DRIFT VELOCITY WITH CURRENT – WITHOUT CURRENT
VS.
DOWN STREAM DISTANCE FROM LEADING EDGE OF BEACH
(From Figure 5)

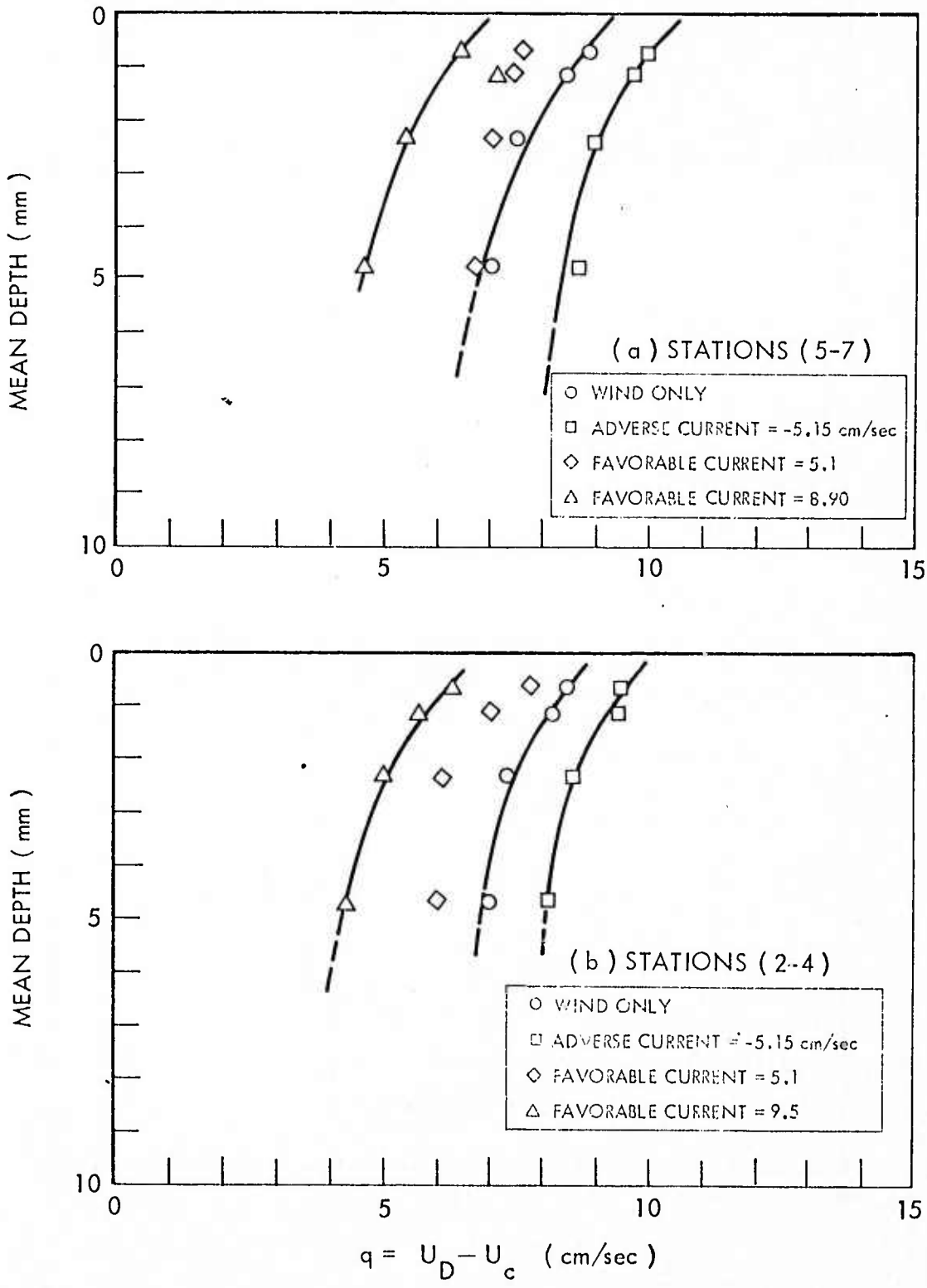

FIGURE 7 - DRIFT CURRENT VS DEPTH , WIND SPEED ≃ 2.75 m / sec
(Data Set B 02, Flat Beach)

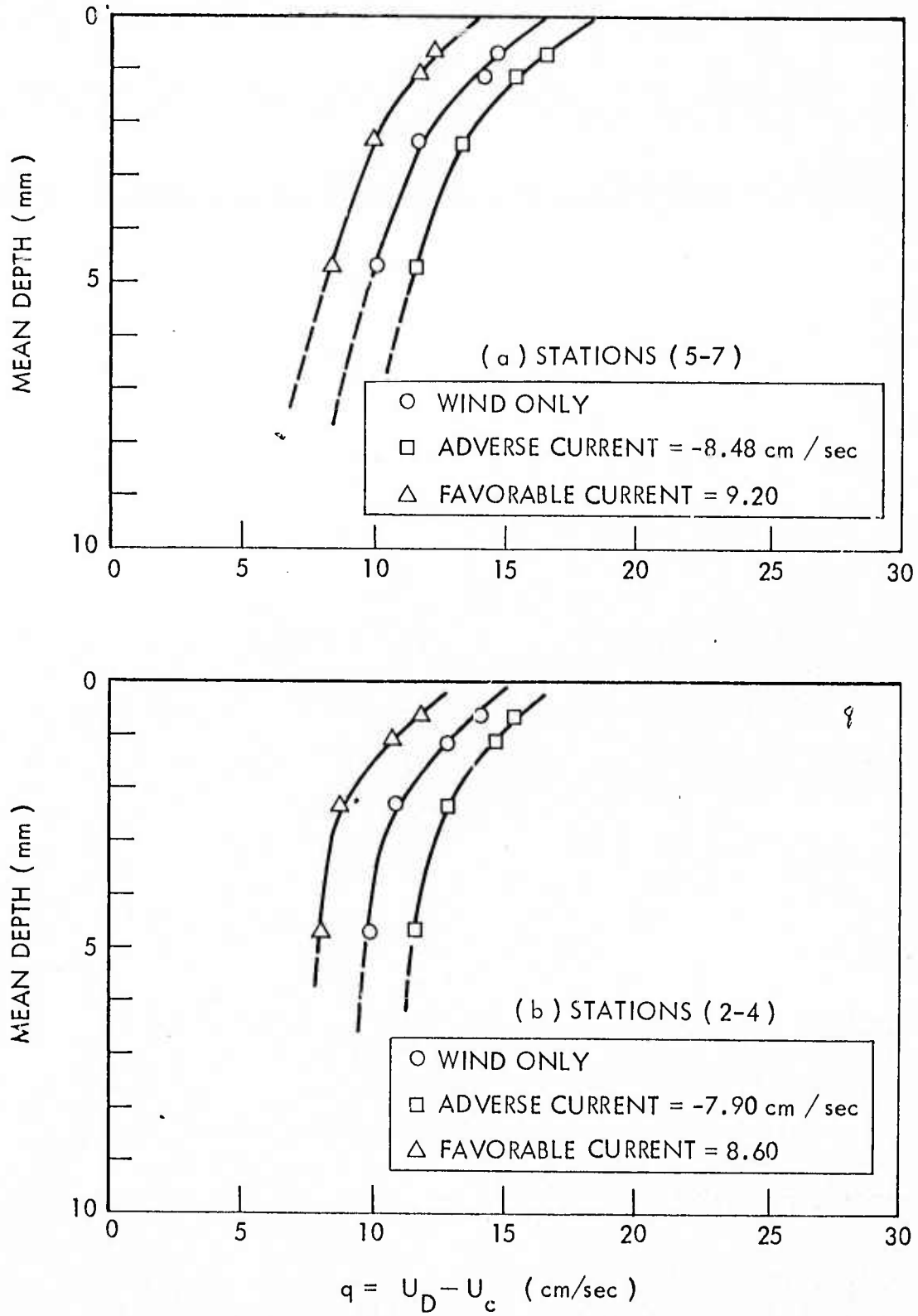

FIGURE 8 - DRIFT CURRENT VS DEPTH, WIND SPEED ≃ 4.75 m/sec
(Data Set B 02, Flat Beach)

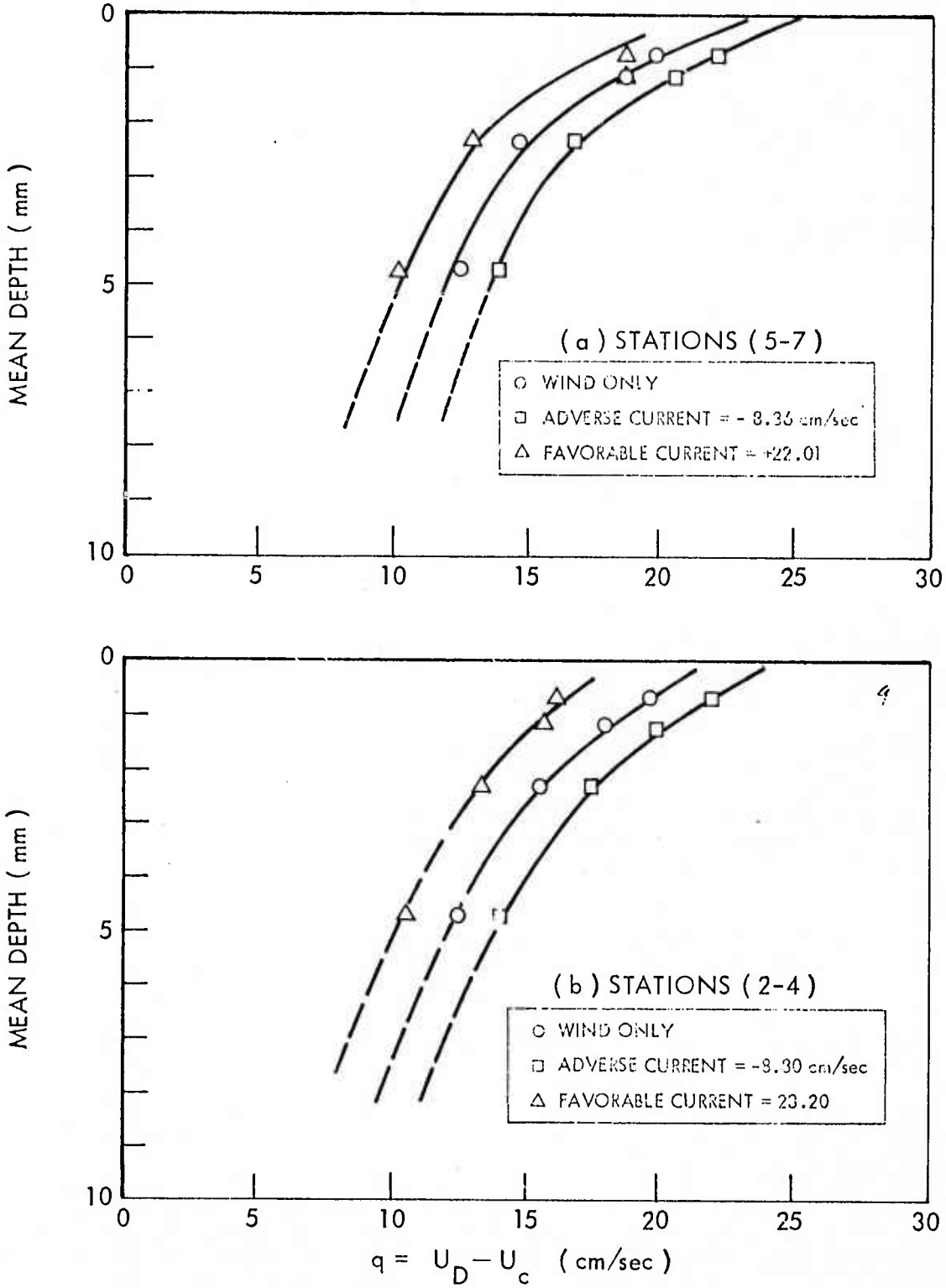

FIGURE 9 - DRIFT CURRENT VS DEPTH, WIND SPEED ≈ 6.67 m/sec
(Data Set B 02, Flat Beach)

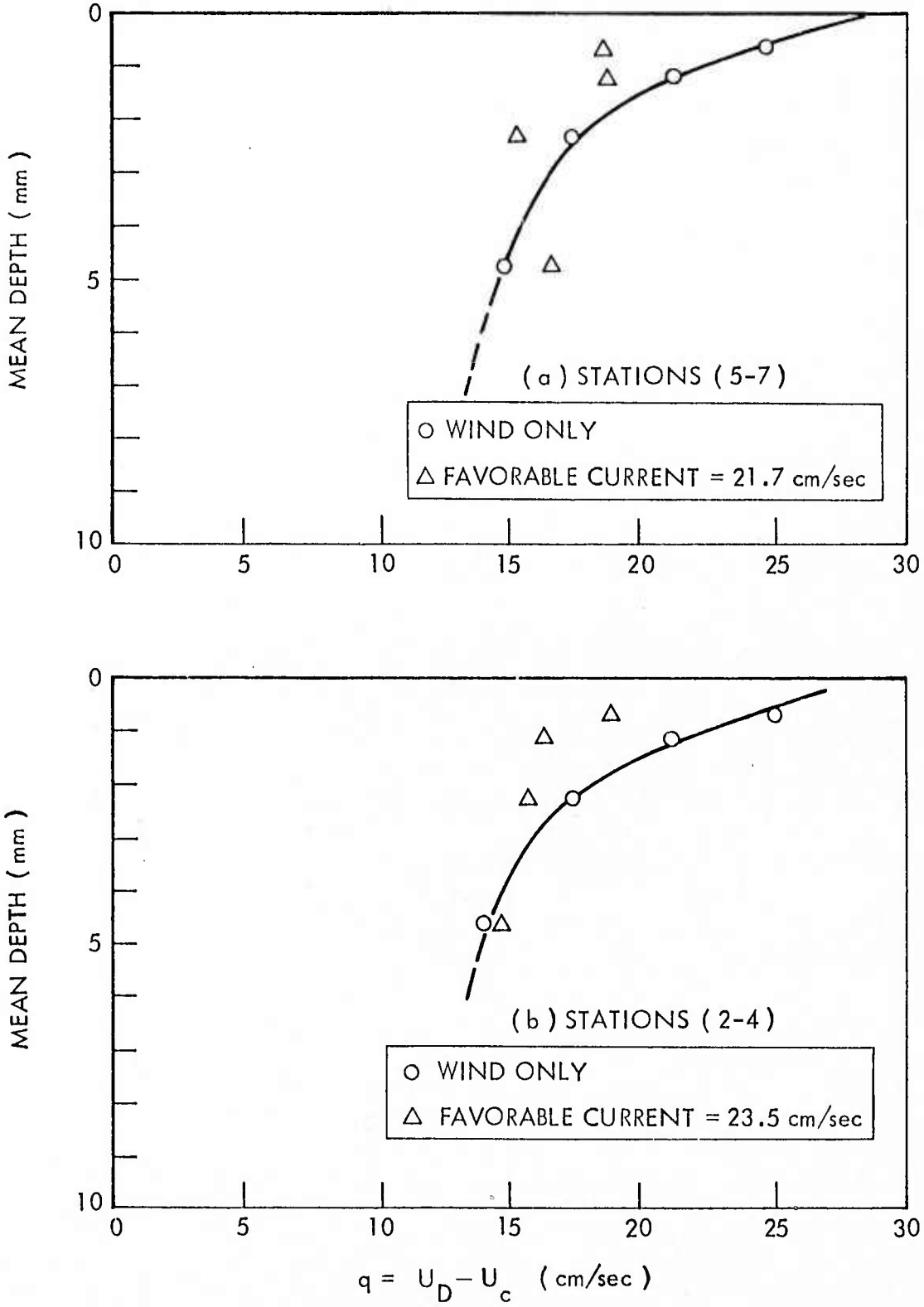

FIGURE 10 - DRIFT CURRENT VS DEPTH, WIND SPEED ≃ 7.65 cm/sec
(DATA SET B02, FLAT BEACH)

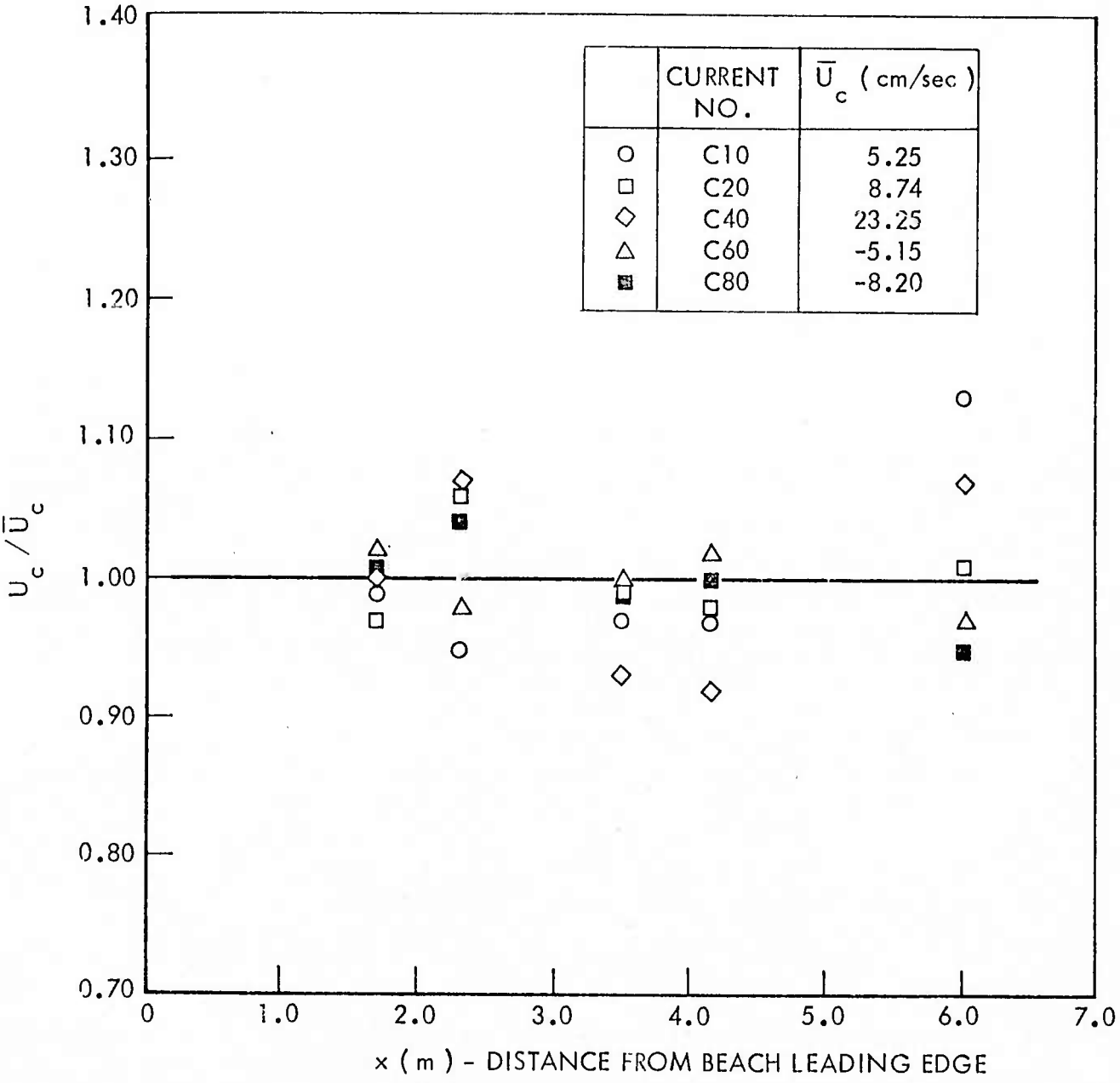

FIGURE 11 - SUBSURFACE CURRENTS AS MEASURED ALONG HORIZONTAL BEACH
(DATA SET B02, FLAT BEACH)

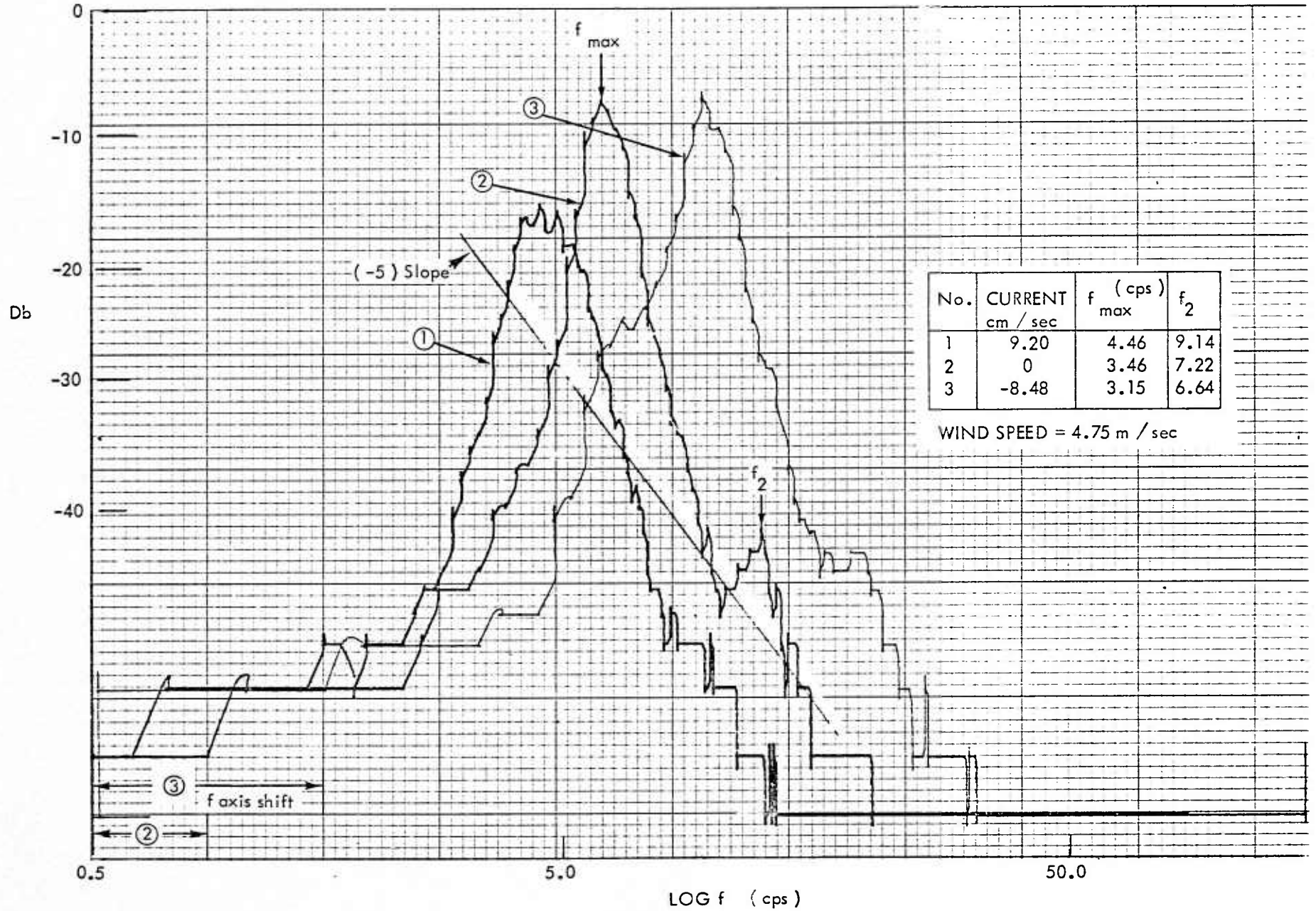

FIGURE 12 - WAVE HEIGHT - ENERGY SPECTRA AT STATION 6
(DATA SET B02, FLAT BEACH)

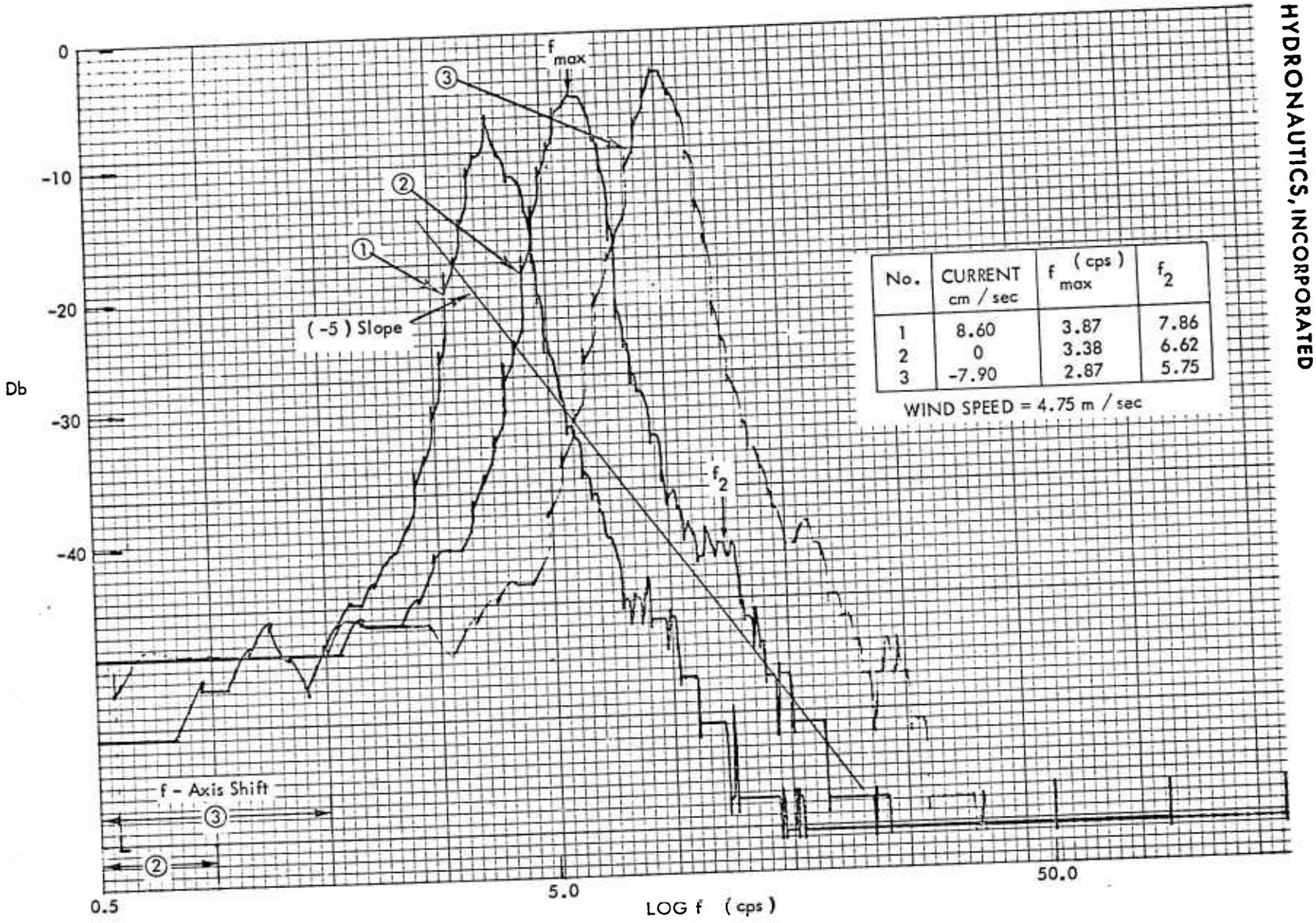

FIGURE 13 - WAVE HEIGHT - ENERGY SPECTRA AT STATION 6. (Data Set B 02, Flat Beach)

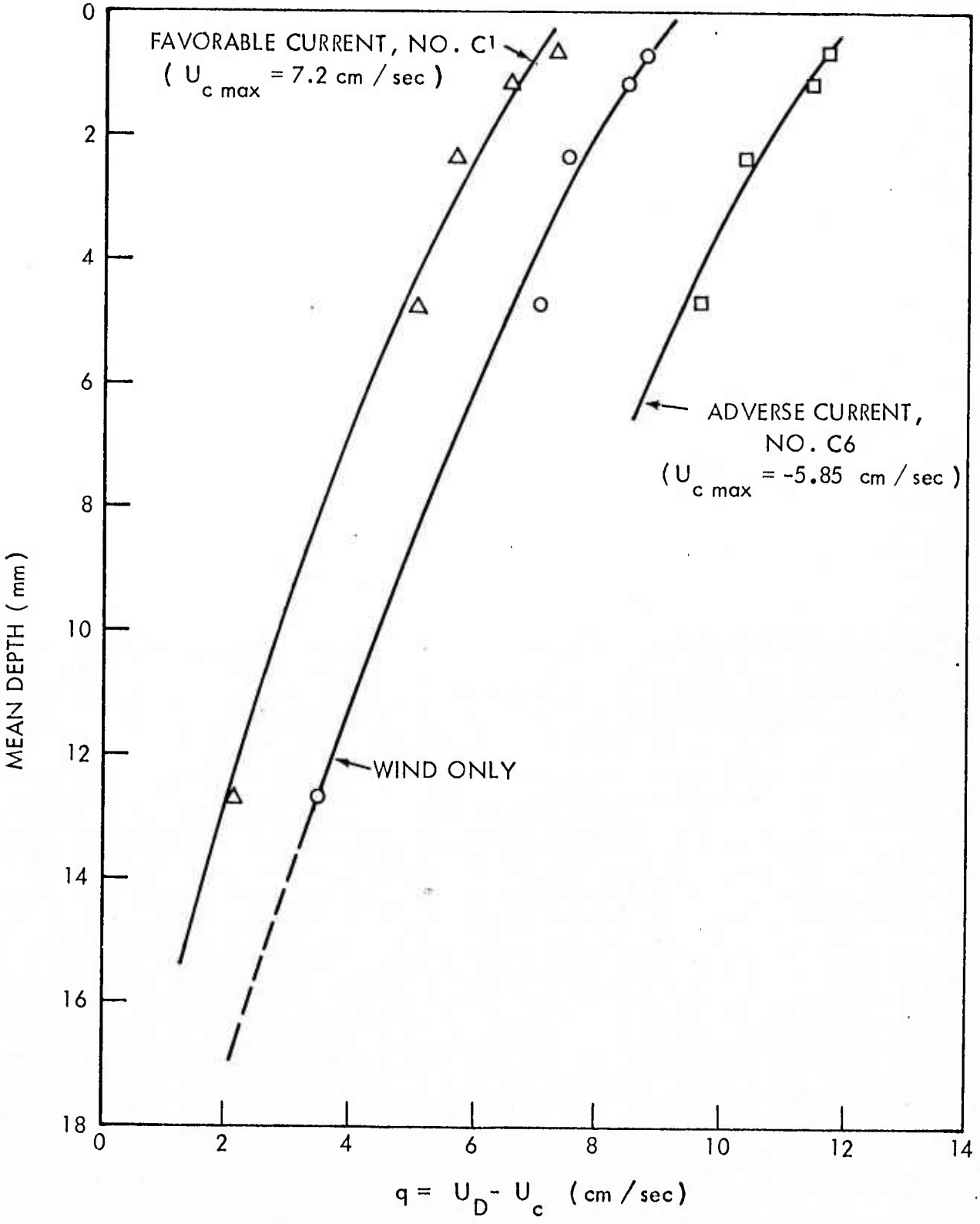

FIGURE 14 - DRIFT CURRENT VS. DEPTH AT STN 6, WIND SPEED ≃ 2.75 m/sec
(DATA SET B4, BEACH ANGLE = 2.65°)

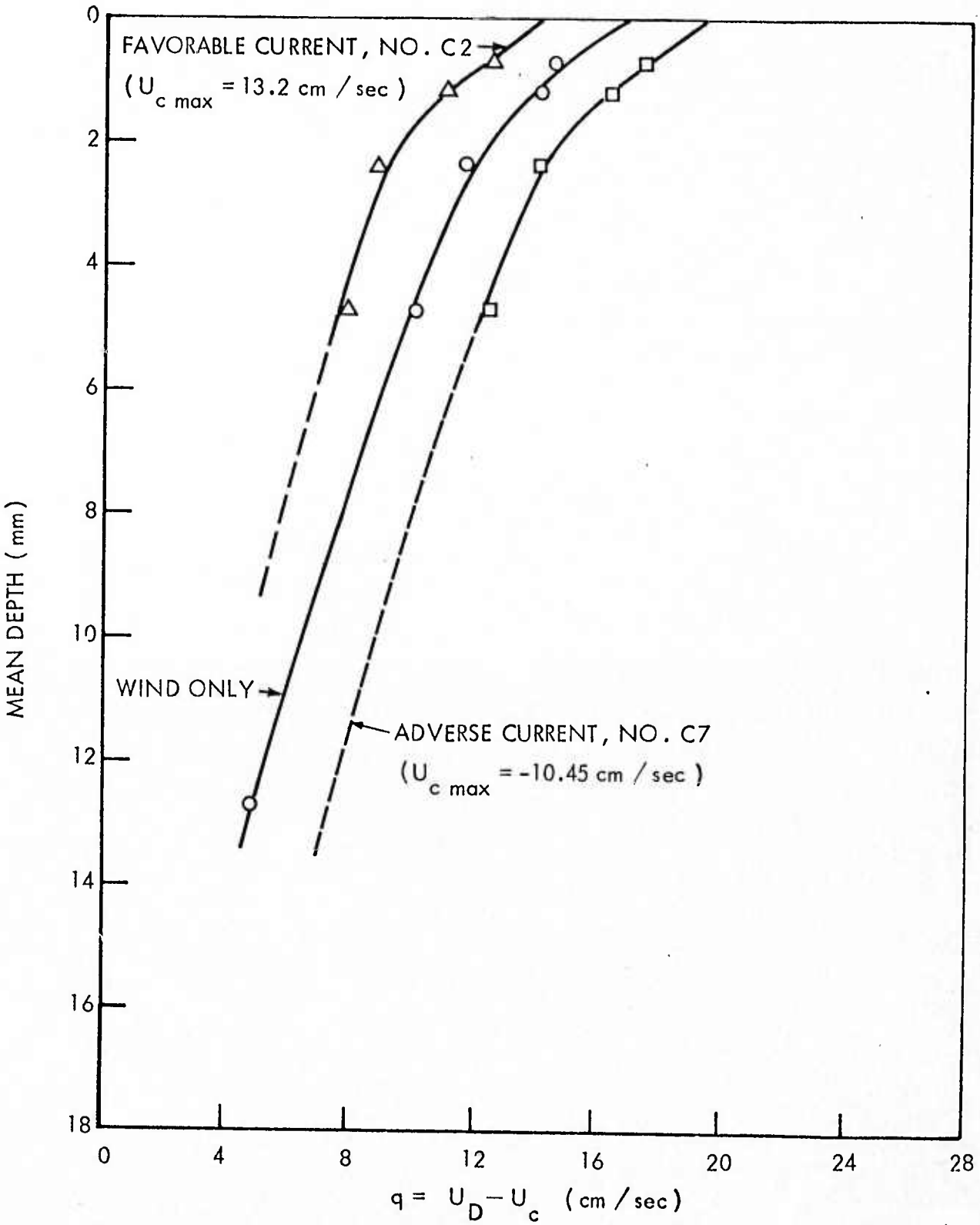

FIGURE 15 - DRIFT CURRENT VS. DEPTH AT STN 6, WIND SPEED ≈ 4.75 m /sec
(DATA SET B4, BEACH ANGLE = 2.65°)

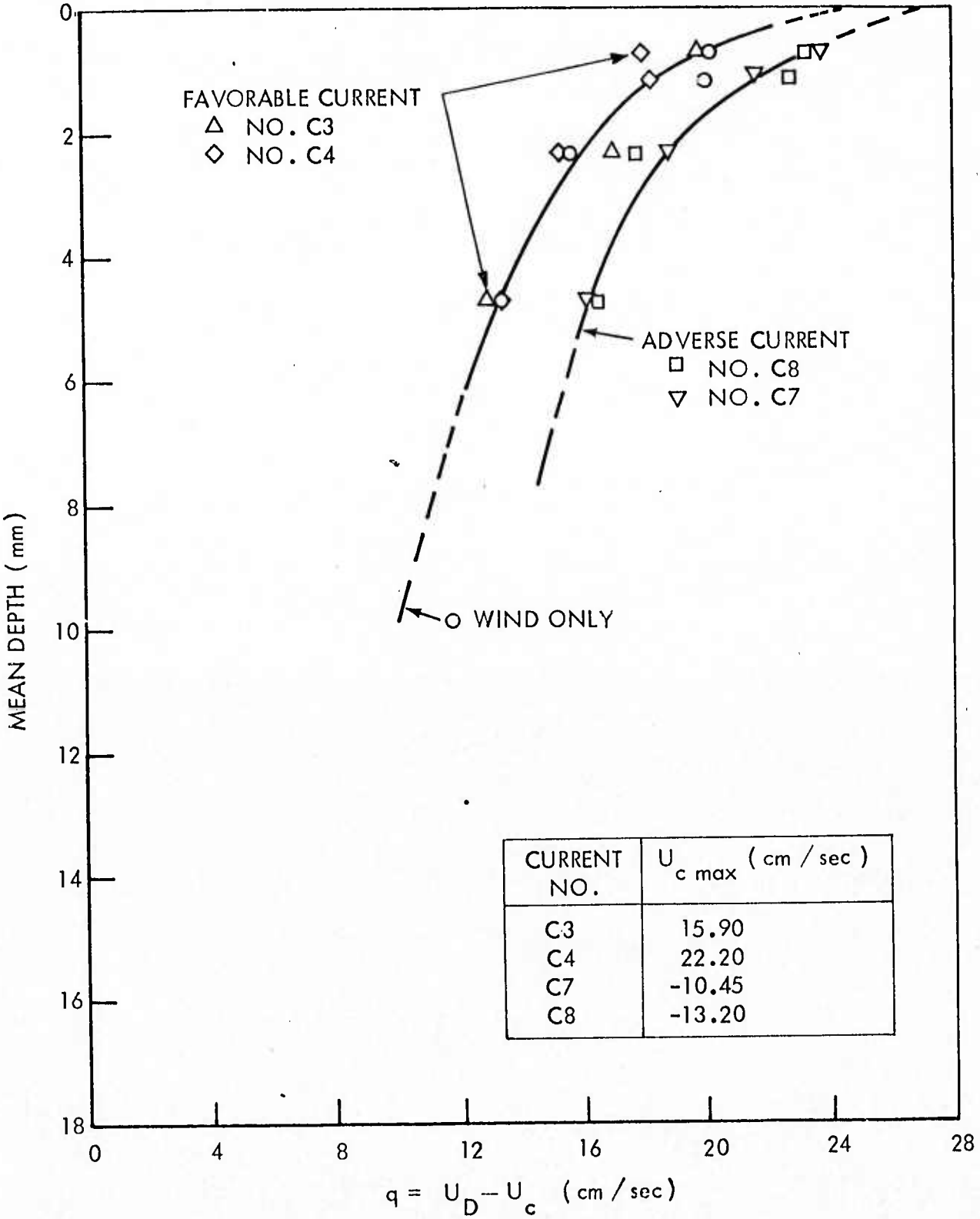

CURRENT NO.	$U_{c\ max}$ (cm / sec)
C3	15.90
C4	22.20
C7	-10.45
C8	-13.20

FIGURE 16 - DRIFT CURRENT VS. DEPTH AT STN 6, WIND SPEED ≃ 6.67 m / sec
(DATA SET B4, BEACH ANGLE = 2.65°)

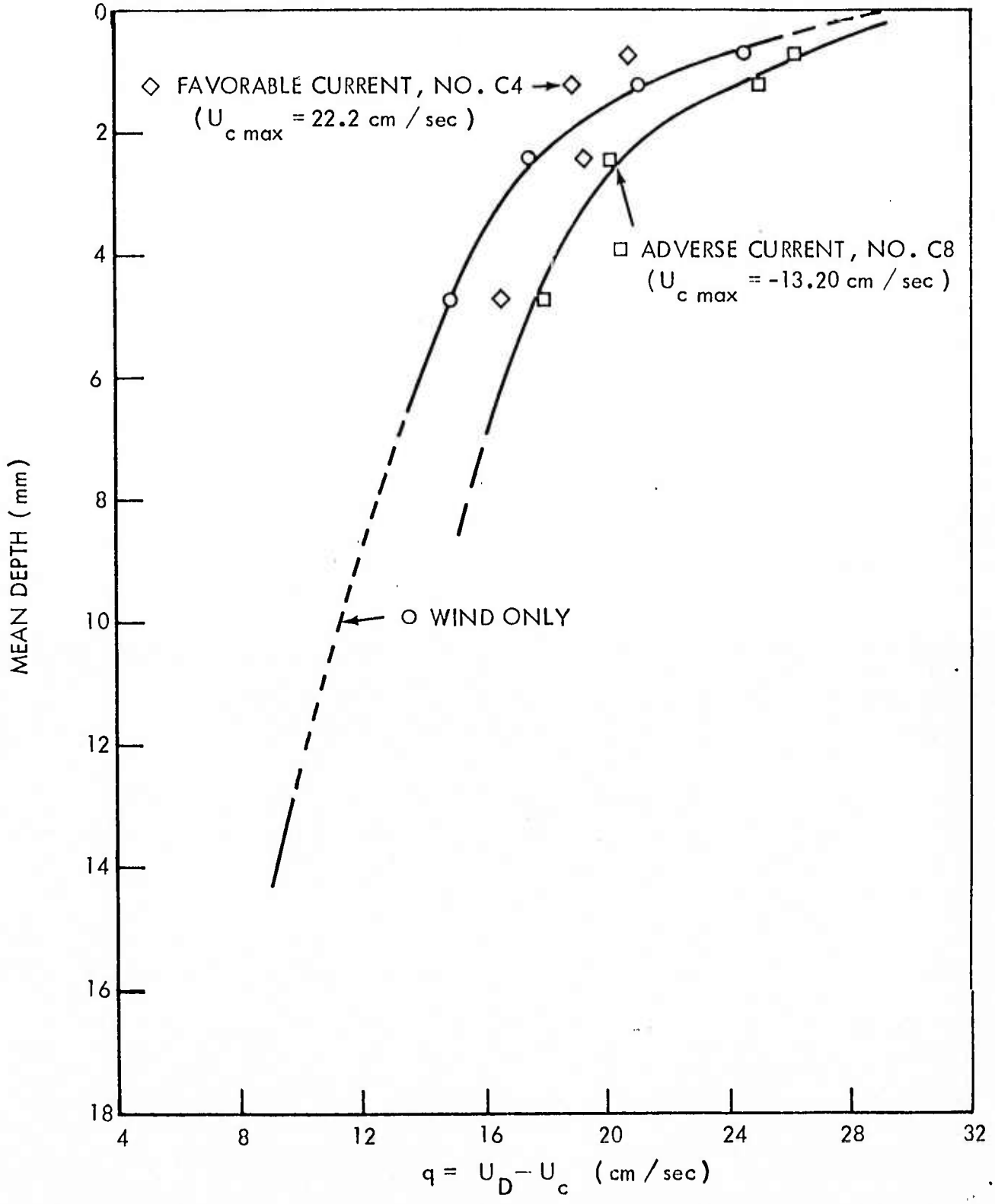

FIGURE 17 - DRIFT CURRENT VS. DEPTH AT STN 6, WIND SPEED ≈ 7.65 m / sec
(DATA SET B4, BEACH ANGLE = 2.65°)

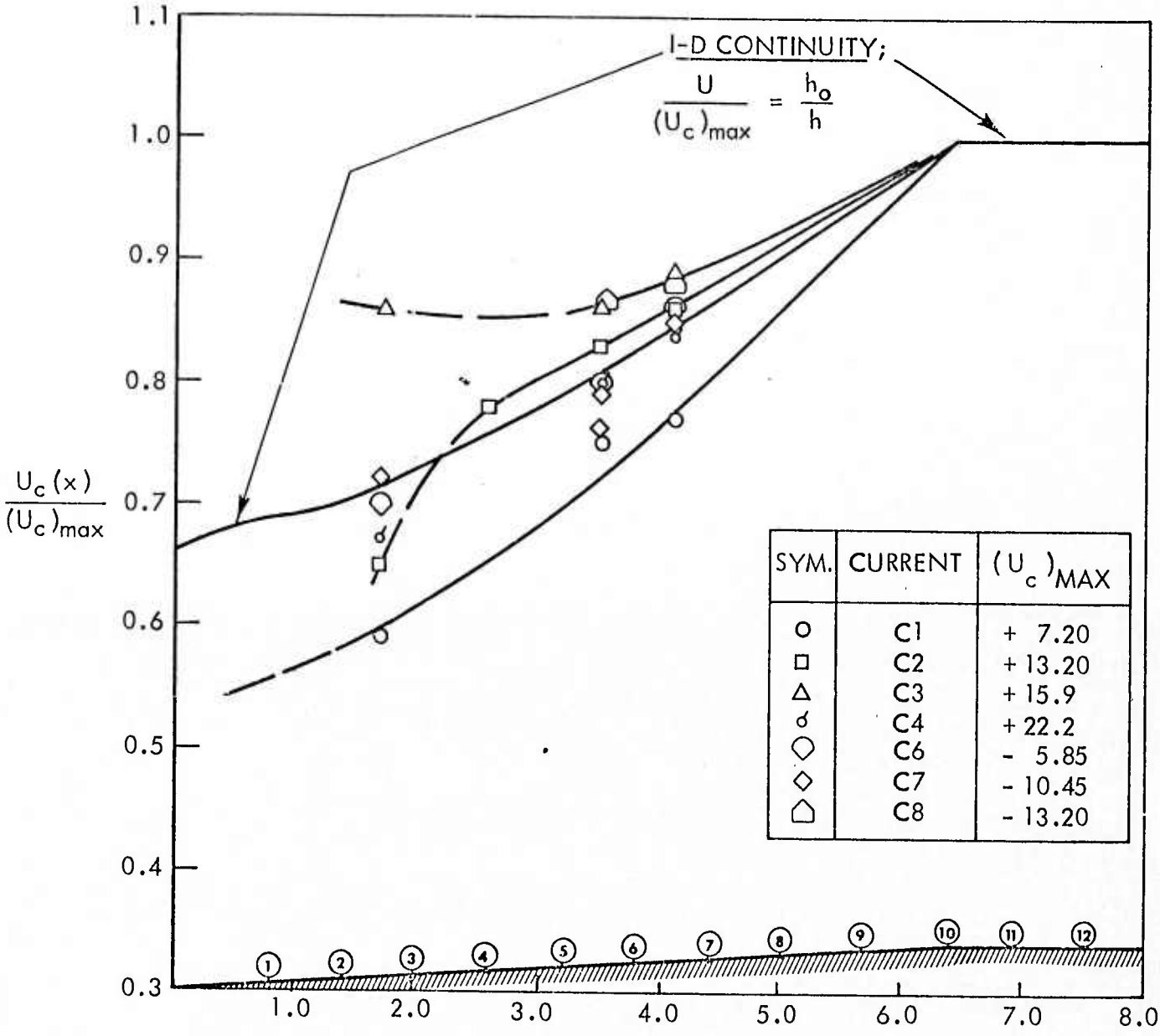

FIGURE 18 - CURRENT ALONG BEACH. (Data Set B4, Beach at 2.65°)

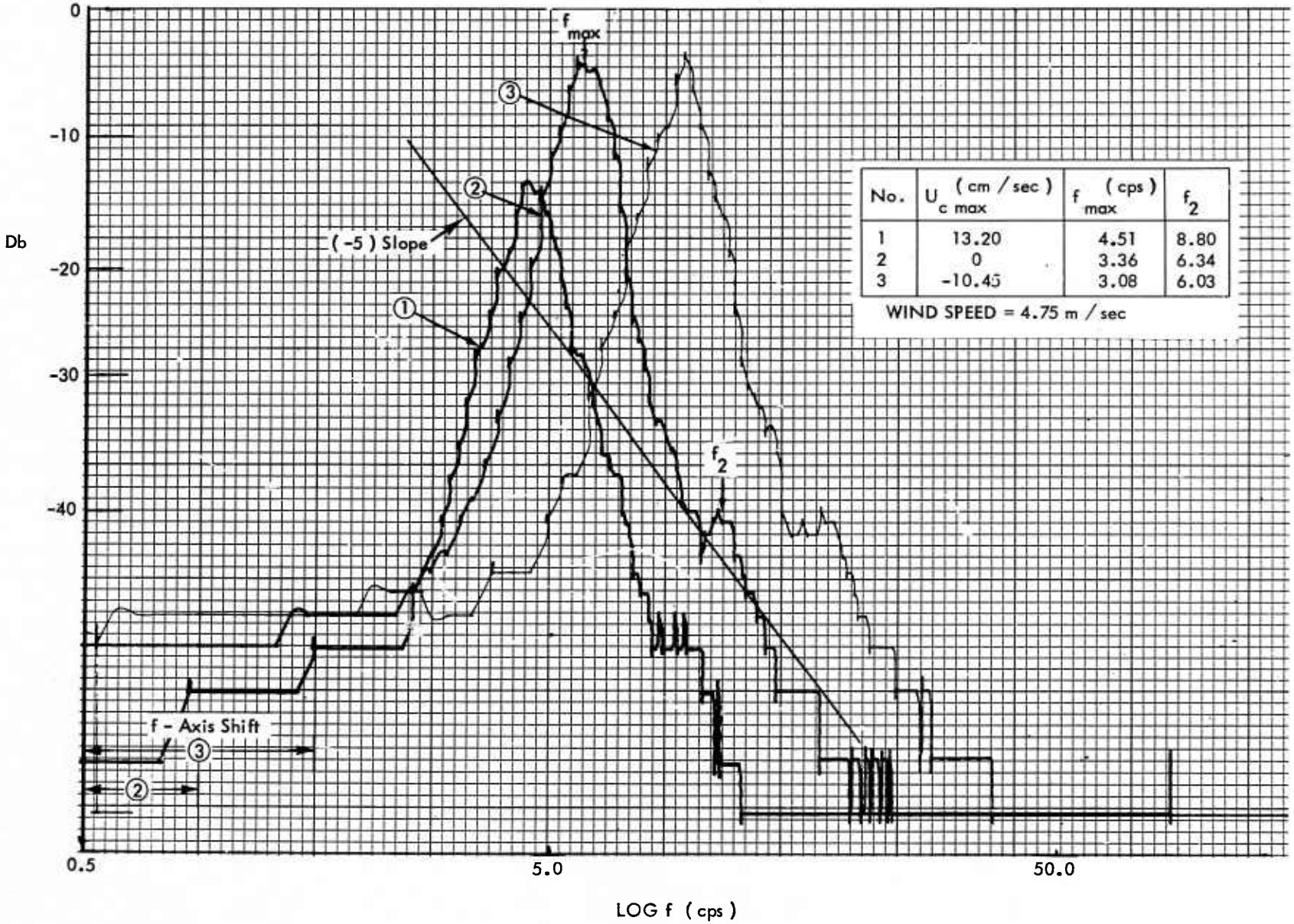

No.	$U_{c\ max}$ (cm / sec)	f_{max} (cps)	f_2
1	13.20	4.51	8.80
2	0	3.36	6.34
3	-10.45	3.08	6.03

WIND SPEED = 4.75 m / sec

FIGURE 19 - WAVE HEIGHT - ENERGY SPECTRA AT STATION 6
(DATA SET B4, BEACH AT 2.65°)

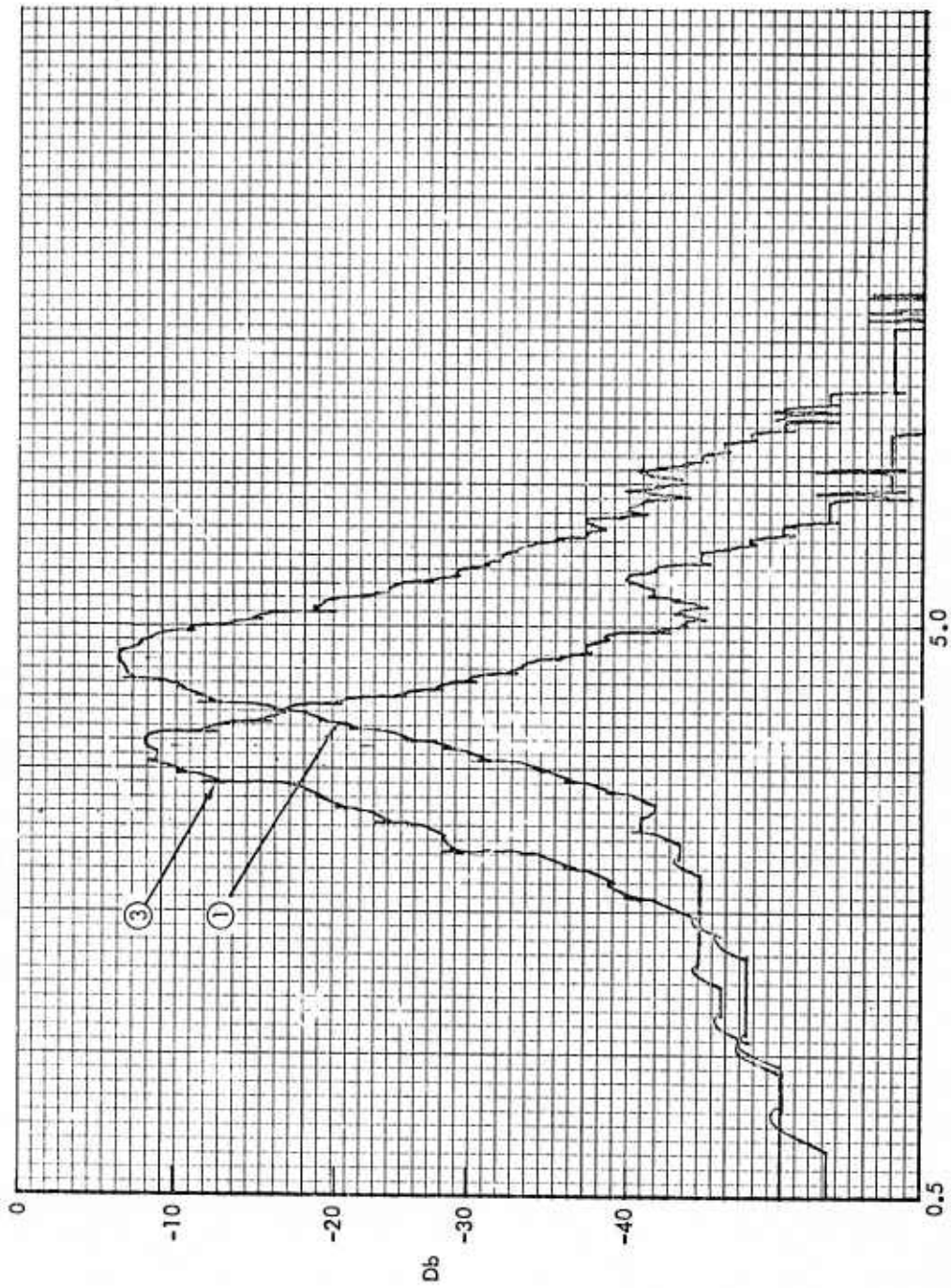

FIGURE 20 - WAVE HEIGHT - ENERGY SPECTRA AT STATION 6. (From Figure 19)

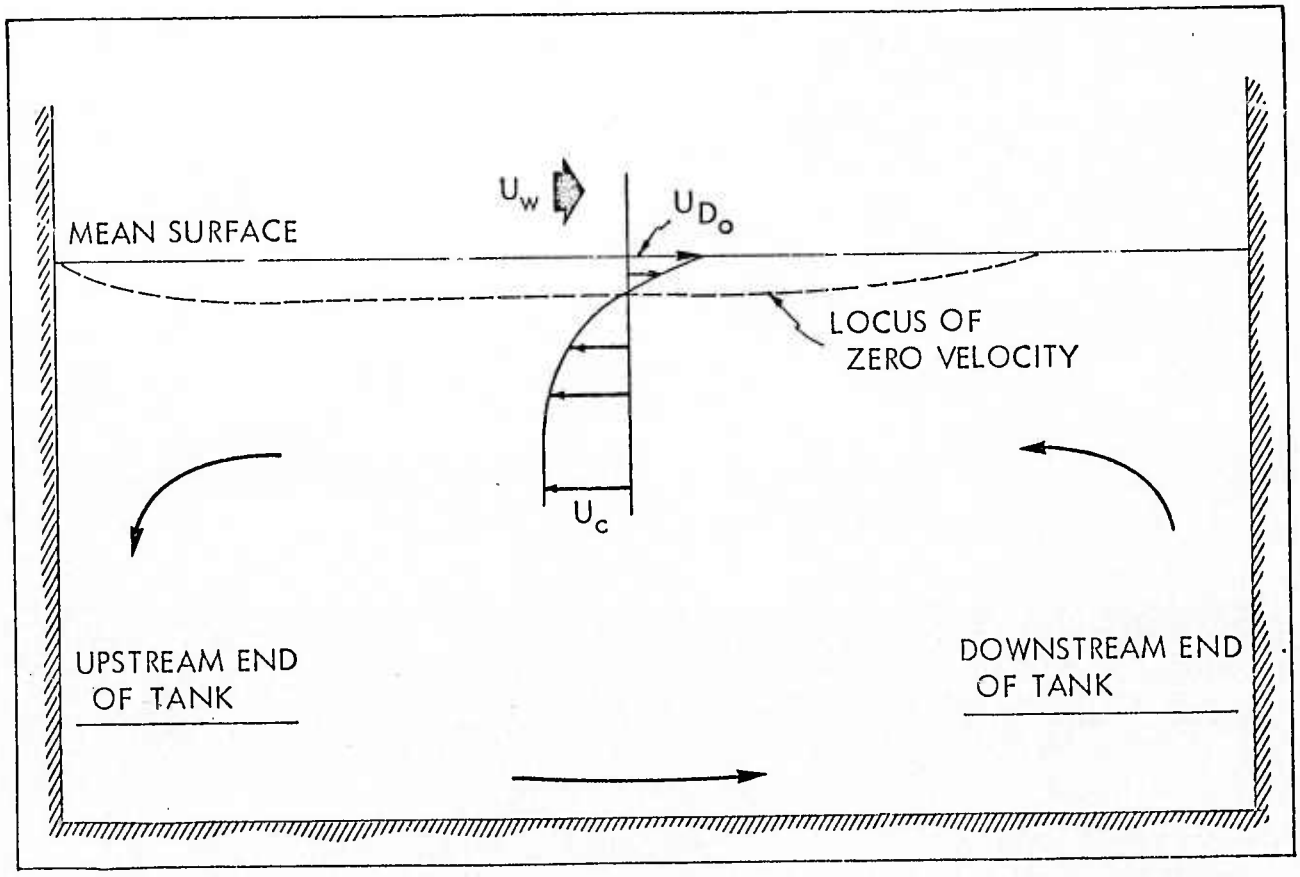

FIGURE 21 - SCHEMATIC OF FLOW FIELD GEOMETRY FOR THE CASE OF WIND PLUS ADVERSE CURRENT

HYDRONAUTICS, Incorporated

DISTRIBUTION LIST
Contract No. N00014-72-C-0509
NR 062-472

Dr. J. D'Albora
Naval Undersea Systems Center
Newport RI 02840 1

Johns Hopkins University
Applied Physics Laboratory
8621 Georgia Avenue
Silver Spring MD 20910
Attn: L. Cronvich 1
H. Gilreath 1
A. Stone 1

University of California,
San Diego
Marine Physical Lab. of the
Scripps Inst. of Oceanography
San Diego CA 92152
Attn: Dr. F. Spiess 1
Dr. T. Foster 1

University of California
San Diego
P. O. Box 119
La Jolla CA 92038
Attn: Dr. W. Nierenberg 1
Dr. W. Munk 1
Dr. C. Cox 1
Dr. R. Davis 1
Dr. C. Gibson 1
Dr. J. Miles 1

Dr. Martin H. Bloom
Polytechnic Inst. of Brooklyn
Route 110, Room 205
Farmingdale NY 11735 1

Dr. Harold W. Lewis
Inst. for Defense Analysis
P. O. Box 6234
Santa Barbara CA 93111 1

Dr. Fredrick Zachariasen
Sloan Laboratory
California Inst. of Tech.
1201 E. California Blvd.
Pasadena CA 91108 1

General Research Corporation
1501 Wilson Blvd.
Suite 700
Arlington VA 22209
Attn: S. Kelly 1

Riverside Research Institute
80 West End Avenue
New York NY 10023
Attn: Dr. Marvin King 1

Dr. P. Chan
Science Applications, Inc.
P. O. Box 2351
La Jolla CA 92037 1

Tetra Tech, Inc.
630 N. Rosemead Blvd.
Pasadena CA 91107
Attn: Dr. M. Todd 1

University of California
Lawrence Radiation Laboratory
P. O. Box 808
Livermore CA 94550
Attn: Dr. R. N. Keele 1

Dr. Coleman duP. Donaldson
Aeronautical Research Associates
of Princeton, Inc.
50 Washington Road
Princeton NJ 08540 1

R & D Associates
P. O. Box 3580
Santa Monica CA 90403
Attn: Dr. D. Holliday 1
Dr. M. Milder 1
Dr. J. Chapyak 1

Aerospace Corporation
P. O. Box 5866
San Bernardino CA 92408
Attn: Dr. Thomas Taylor 1

TRW Systems Group
One Space Park
Redondo Beach CA 90278
Attn: Dr. J. Chang 1
Dr. E. Baum 1

Dr. Frank Lane
KLD Associates, Inc.
7 High Street
Suite 204
Huntington NY 11743 1

Dr. Michael Y. H. Pao
Flow Research, Inc.
1819 S. Central Avenue
Suite 72
Kent WA 98031 1

HYDRONAUTICS, Incorporated
7210 Pindell School Rd.
Howard Co.
Laurel MD 20810
Attn: Mr. M. Tulin 1
Dr. T. R. Sundaram 1

Xonics, Inc.
6837 Hayvenhurst Avenue
Van Nuys CA 91406
Attn: Dr. Balser 1

Physical Dynamics, Inc.
P. O. Box 1069
Berkeley CA 94704
Attn: Dr. Bruce West 1
Dr. J. Alex Thomson 1

Dr. Roberto Vaglio-Laurin
Advanced Tech. Labs., Inc.
400 Jericho Turnpike
Jericho NY 11753 1

California Inst. of Tech.
1201 E. California Blvd.
Pasadena CA 91109
Attn: Dr. Toshi Kubota 1
Dr. Milton Plesset 1

Cornell Aeronautical Lab., Inc.
4455 Genesee Street
Buffalo NY 14221
Attn: H. Radt 1

Stanford Research Institute
333 Ravenswood Avenue
Menlo Park CA 94025
Attn: H. Guthardt 1
K. Kirshnan 1

Mr. J. McCarthy
Naval Ship Research and
Development Center
Washington, D. C. 20084 1

Dr. G. F. Carrier
Harvard University
Pierce Hall
Cambridge MA 02138 1

Institute for Advanced Study
Princeton NJ 08549
Attn: Dr. Roger Dashen 1
Dr. M. Rosenbluth 1

Dr. Curtis Callan, Jr.
Princeton University
Dept. of Physics
Princeton NJ 08540 1

Dr. C. M. Tchen
1380 Riverside Drive
New York NY 10033 1

Dr. J. Menkes
University of Colorado
Boulder CO 80302 1

Inst. for Defense Analysis
400 Army-Navy Drive
Arlington VA 22202
Attn: Dr. Phillip A. Selwyn 1
Mr. J. C. Nolen 1

U.S. Naval Research Laboratory
Washington, D. C. 20390
Attn: Frank MacDonald 1
J. O. Elliot 1
K. G. Williams 1
A. Berman 1
S. Piacsek 1
J. Witting 1

Office of Naval Research
Department of the Navy
Washington, D. C. 20360
Attn: M. Cooper 1
R. Cooper 1

Naval Undersea Research and
Development Center
San Diego CA 92132
Attn: Library 1

Advanced Research Projects Agency
1400 Wilson Blvd.
Arlington, VA 22209
Attn: Bruce James 1
F. Koether, TIO 1

CIA, Headquarters
Mclean, VA
Attn: H. Farmer 1

James H. Probus (OASN)
Room 4E741
The Pentagon
Washington, D. C. 20350 1

Cdr. Don Walsh (OASN/R&D)
Room 4E741
The Pentagon
Washington, D. C. 20350 1

SP202
Department of the Navy
Washington, D. C. 20390 1

Dr. D. A. Rogers (NSP)
SP2018
Department of the Navy
Washington, D. C. 20390 1

Dr. J. B. Hersey
Bldg. 58
Naval Research Laboratory
Washington, D. C. 20390 1

Naval Ship Systems Command
TRIDENT Project Officer
Washington, D. C. 20360 1

Naval Scientific and Technical
Intelligence Center
Attn: Capt. J. P. Prisley
4301 Suitland Road
Washington, D. C. 20390 1

Naval Air Systems Command
I. H. Gatzke
Main Navy Bldg.
Washington, D. C. 20360 1

Dr. K. Saunders
Pacific-Sierra Research Corp.
1456 Clover Field Blvd.
Santa Monica CA 90404 1

Defense Documentation Center
Cameron Station
Alexandria VA 22314 12